



City Research Online

City, University of London Institutional Repository

Citation: Qian, K., Liang, S-L., Fu, F. & Fang, Q. (2019). Progressive Collapse Resistance of Precast Concrete Beam-Column Sub-assemblages with High-Performance Dry Connections. *Engineering Structures*, 198, 109552. doi: 10.1016/j.engstruct.2019.109552

This is the accepted version of the paper.

This version of the publication may differ from the final published version.

Permanent repository link: <https://openaccess.city.ac.uk/id/eprint/22657/>

Link to published version: <https://doi.org/10.1016/j.engstruct.2019.109552>

Copyright: City Research Online aims to make research outputs of City, University of London available to a wider audience. Copyright and Moral Rights remain with the author(s) and/or copyright holders. URLs from City Research Online may be freely distributed and linked to.

Reuse: Copies of full items can be used for personal research or study, educational, or not-for-profit purposes without prior permission or charge. Provided that the authors, title and full bibliographic details are credited, a hyperlink and/or URL is given for the original metadata page and the content is not changed in any way.

City Research Online:

<http://openaccess.city.ac.uk/>

publications@city.ac.uk

1
2 **Progressive Collapse Resistance of Precast Concrete Beam-Column Sub-**
3 **assemblages with High-Performance Dry Connections**

4 Kai Qian^{1*}, Shi-Lin Liang¹, Feng Fu², and Qin Fang³

5 ¹ College of Civil Engineering and Architecture, Guangxi University, 100 Daxue Road, China, 530004.

6 ² School of Mathematics, Computer Science and Engineering, Northampton Square, London, EC1V 0HB, U.K.

7 ³ Army Engineering University, Nanjing 210007, Jiangsu, Peoples R China

8 **Abstract:** Due to its relatively lower integrity, precast concrete structures are considered to be more
9 vulnerable to progressive collapse than cast-in-place concrete structures. However, to date, majority
10 of existing studies on progressive collapse focused on cast-in-place concrete structures, little
11 attentions were paid to precast concrete structures. Among existing precast concrete structures,
12 unbonded post-tensioning precast concrete structure is one of innovation dry connection structural
13 systems, which no casting at the connections on site. Its excellent seismic performance was
14 recognized by many studies, while studies on its progressive collapse resistance were very few. To
15 fill this knowledge gaps, in this paper, eight half-scaled unbonded post-tensioning precast concrete
16 beam-column sub-assemblages with different connection configurations were tested through
17 pushdown tests to investigate their capacities and resistance mechanisms to prevent progressive
18 collapse. The test results demonstrated various behaviors of beam-column sub-assemblages with
19 different connection types. It was found that, as the longitudinal reinforcements were discontinuous
20 across the beam-column joint region in the beams, flexural action observed in the cast-in-place
21 concrete frames was not mobilized for the specimens with purely unbonded post-tensioning
22 connections. When the specimens installed top-seat angles at the beam-column interfaces,
23 considerable flexural action capacity could be mobilized for load resistance. Moreover, it was found
24 that the failure modes of the specimens are distinctly different to that of conventional reinforced
25 concrete frames or precast concrete frames with cast-in-place joints. The characteristic of
26 compressive arch action and tensile catenary action in tested specimens is quite different to that of
27 conventional reinforced concrete frames.

29

30 **1. Introduction**

31 Due to the advantages of environment friendly, fast track construction, large bulk of offsite
32 production, and high-quality workmanships, precast concrete (PC) structures are widely used in the
33 construction projects worldwide. However, as the beam longitudinal reinforcements are
34 discontinuous in the beam-column joint, PC frames with normal dry connections are more vulnerable
35 to progressive collapse, compared to conventional cast-in-place reinforced concrete (RC) frames. To
36 date, majority of attentions were paid on monolithic cast-in-place RC structures to resist progressive
37 collapse. Su et al. [1] tested twelve 1/2 scaled specimens to investigate the effects of beam
38 reinforcement ratio, span-to-depth ratio, and loading rate on compressive arch action (CAA) capacity
39 of RC beam-column sub-assembly. Sadek et al. [2] tested two full-scale RC sub-assemblies with
40 different seismic details. Yu and Tan [3] experimentally investigated the effects of seismic design on
41 the performance of RC frames in mitigating progressive collapse. Yu and Tan [4] proposed three
42 special detailing to enhance the progressive collapse resistance of RC frames. Ren et al. [5] and Lu et
43 al. [6] carried out a series of tests on beam-slab and beam-column sub-assemblies subjected to edge
44 or middle column missing scenario to investigate the contribution of RC slabs in progressive collapse
45 resistance. Qian et al. [7] discussed the contribution of each alternate load path of RC buildings, such
46 as CAA, tensile catenary action (TCA), and compressive/tensile membrane action to resist
47 progressive collapse. Qian and Li [8-9] filled knowledge gaps for RC frames subjected to the loss of
48 a corner column. Meanwhile, the benefits from slab to resist progressive collapse were quantified by
49 Qian and Li [10-11]. It was found that the RC slab could significantly improve the behavior of RC
50 buildings against progressive collapse. Shan et al. [12] tested two 1/3 scale, four-bay by two-story
51 RC planar frames to investigate the effects of infilled wall on the load resisting mechanisms of RC
52 frames. It was found that the infill walls could enhance the load resisting capacity of frames
53 significantly. Peng et al. [13-14] experimentally evaluated the dynamic response of flat plate

54 structure subjected to an exterior or interior column removal scenario. Ma et al. [15] tested a 1/3
55 scaled RC flat plate substructure to assess its behavior under a corner column removal scenario. Qian
56 et al. [16] investigated the advantages of using steel braces to strengthen the progressive collapse
57 resistance of RC frames. The steel brace increased the initial stiffness and CAA capacity significantly
58 whereas few benefits for TCA were observed, due to compressive buckling or tensile fracture in
59 braces at large displacement stage. Sasani et al. [17-21] conducted a series of on-site tests to capture
60 the behavior of RC multi-storey structure subjected to different initial damages. These on-site tests
61 evaluated the load resisting contribution from Vierendeel action, flexural action, and non-structural
62 element such as infill walls. However, studies on PC frames to resist progressive collapse were very
63 few. Nimse et al. [22] studied the progressive collapse behavior of PC beam-column sub-assemblages
64 with monolithic joints. Kang and Tan [23] experimentally investigated the effects of joint
65 reinforcement detailing and reinforcement ratio on load resistance of PC beam-column sub-
66 assemblages. Kang and Tan [24] test four specimens to assess the robustness of PC frames subjected
67 to the loss of a penultimate column scenario. It was found that, with reasonable anchorage details, the
68 PC structures with cast-in-place topping could obtain similar behavior as RC structures. Keyvani [25-
69 26] conducted studies on behavior of precast prestressed concrete flat slab floor to resist progressive
70 collapse. It was found that bonded post-tensioned floor system was more susceptible to failure after
71 column removal than unbonded one due to localization of tendon strains. Qian and Li [27] tested two
72 large-size PC and beam-column-slab substructures with monolithic joints and one reference RC
73 substructure to investigate the load resisting mechanism of PC frames. It was indicated that CAA,
74 TCA could be developed in PC beams and compressive/tensile membrane actions could be developed
75 in PC hollow core slabs with cast-in-place topping layer. However, it should be noted that PC
76 construction with cast-in-place monolithic joints (wet joints) could not reflect the advantage of PC
77 construction sufficiently. Therefore, the performance of PC frames with dry connections to mitigate
78 progressive collapse was investigated by Al-Salloum et al. [28], Quiel et al. [29], and Qian and Li
79 [30]. These tests indicated that PC frames with welded connection could not develop TCA owing to
80 the early failure of the welded connection. The PC frames with bolted connection could not develop

81 CAA in PC beams as the gap between the beam and column allows the PC beams to expand outward.
82 The bolted connection could prevent the PC beams to develop TCA, as the reinforcements were
83 discontinuous at the beam-column joints.

84 From above existing studies, it can be seen that, it is imperative to evaluate the robustness of PC
85 frames with other types of dry connections to resist progressive collapse. PC frames with unbonded
86 post-tensioning (UPT) strands were one of innovative dry connections, which was initially proposed
87 by PREcast Seismic Structural System (PRESSSS) program. A number of tests [31-32] had been
88 carried out for the evaluation of the seismic behavior of PC frames with UPT strands. It was found
89 that the PC frames with UPT strands could provide desirable load carrying and deformation capacity
90 with little residual damage. However, the PC frame with UPT strands has low energy dissipation
91 capacity. Therefore, to enhance the energy dissipation capacity of the system, several studies were
92 conducted. Santon et al. [33] and stone et al. [34] placed extra mild rebar grouted in ducts in the
93 beam-column joints regions to dissipate extra energy (hybrid system). It was found that the load
94 resistance and energy dissipation capacity of the hybrid systems can match that of cast-in-place RC
95 system. Then, Rodgers et al. [35-36] proposed new energy dissipation devices for hybrid system.
96 Song et al. [37-38] conducted a series of tests on a novel hybrid connection. In such a connection,
97 steel jackets were installed at the beam ends to achieve damage avoidance. The test results revealed
98 favorable reparability in addition to self-centering and energy dissipation capacity of the novel
99 connection. However, the aforementioned studies were mainly focused on the performance of the PC
100 system with UPT strands or hybrid system subjected to cyclic load. Few studies were carried out to
101 investigate their resistance to progressive collapse (monotonic load). Therefore, in this paper, a series
102 of eight one-half scaled PC beam-column substructures with three different types of connections
103 (UPT connection, hybrid connection with additional bolted top-seat angle, and pure bolted top-seat
104 angle connection for comparison purpose) were tested under quasi-static pushdown loading regime.

105 2. Experimental program

106 Fig. 1 shows the difference of bending moment diagram of a frame before and after removal of a
107 column (interior or penultimate column). It can be seen that, the bending moment in the middle joints

108 above the removed column changed from negative to positive after removal, whereas the negative
109 bending moment at the side joints increased significantly. As this is overlooked in conventional
110 structural design, the structures may suffer severe damage and worth investigating their load
111 redistribution abilities. For this purpose, beam-column sub-assemblages were extracted from the
112 frame at the points of contra-flexure, as shown in Fig. 1b. As shown in the figure, the sub-
113 assemblages subjected to the loss of an interior column (called interior sub-assemblage) or a
114 penultimate exterior column (called exterior sub-assemblage) were investigated for the evaluation of
115 the influence of horizontal constraints on the behavior of PC beam-column sub-assemblages in
116 resisting progressive collapse. The main difference between interior and exterior sub-assemblages
117 was the degree of horizontal constraints at the side columns.

118 **2.1. Test specimens**

119 The prototype building is an eight-storey frame, which was designed in accordance with ACI
120 318-14 [39]. The prototype frame was located on a D class site. The design spectral response
121 acceleration parameters of SDS and SD1 are 0.46 and 0.29, respectively. The design live load of the
122 prototype frame is 2.0 kPa. The dead load including the ceiling weight is 5.1 kPa. Fig. 2 shows the
123 configuration of three different connections: a) UPT connection, b) hybrid connection with additional
124 top-seat angles, c) connected solely by top-seat angles for comparison purpose. Table 1 tabulates the
125 relationship between prototype frame and test specimens, while Table 2 summarized main
126 characteristics of the test specimens. As listed in the Table 2, eight half-scaled specimens, which can
127 be categorized into three groups (UP, TSUP, and TS), were tested. The design variables are
128 connection types, effective prestressing force in strands, and locations of the lost column. UP, TSUP,
129 and TS represent unbounded post-tensioning connection, hybrid connection, and top-seat angle
130 connection, respectively. The letter E and I denote exterior and interior sub-assemblages, respectively.
131 The last numeral denotes effective prestress in unbonded strands. Thus, TSUPE-0.4 indicates an
132 exterior sub-assemblage with effective prestress of $0.4f_{pu}$, which was assembled by hybrid connection,
133 where f_{pu} denotes nominal ultimate strength of the post-tensioning strands (1860 MPa herein). Due to

134 symmetry, only half of the specimen was exhibited in Fig. 3. It should be noted that all specimens
135 have identical cross section of beam and column as well as reinforcement details (refer to Table 1).
136 The nominal diameter and area of unbonded strand are 12.7 mm and 97.8 mm², respectively. The
137 beam longitudinal rebar of 2T12 was placed at both top and bottom layers, which were discontinuous
138 at the joint. 4T16 were used as column longitudinal reinforcement. R6 were used as transverse
139 reinforcement. T12 and T16 denote deformed bars with diameter of 12 mm and 16 mm, respectively,
140 while R6 indicates plain rebar with diameter of 6 mm.

141 ***2.2. Material properties***

142 The concrete used to cast UPE-0.4, UPI-0.4, and UPI-0.65 had an average cylindrical
143 compressive strength of 40.0 MPa and a tensile splitting strength of 3.7 MPa. For the rest of
144 specimens, the cylindrical compressive strength and tensile splitting strength were 38.5 MPa and 3.5
145 MPa, respectively. The material used for top-seat angle was Grade S235, whereas Grade 8.8 M18
146 bolts was employed to fix the top-seat angles with torque of 215 N·m. **The properties of rebar and**
147 **post-tensioning strand were shown in Table 3 and Fig. 4.**

148 ***2.3. Pushdown test setup***

149 The experimental setup is shown in Fig. 5. The side column bottoms were anchored to the pin
150 supports via four high-strength bolts, and then the pin supports were fixed to the strong floor by high
151 strength bolts with diameter of 50 mm. Each overhanging beam was connected to the A-frames
152 through a roller. Moreover, the top of side column was bolted with a steel extension that connected to
153 the A-frame via an additional roller. A self-equilibrium system was employed to apply an axial
154 compressive force at the side column. **A hydraulic jack (Item 1 in Fig. 5a) beneath the H-frame was**
155 **used to apply vertical displacement.** In order to eliminate possible out-of-plane failure of the
156 specimens, a steel assembly (Item 3 in Fig. 5a) was specially designed to provide out-of-plane
157 **restraints** to the specimens.

158 **2.4. Instrumentation**

159 To monitor the structural response accurately, extensive instrumentation was installed to monitor
160 test results. The horizontal reaction forces from column top and overhanging beam were measured by
161 two tension /compression load cells (Item 5 in Fig. 5a), which were installed at the roller. However,
162 a load pin (Item 8 in Fig. 5a), which was installed at the bottom support, was used to measure the
163 horizontal and vertical reaction forces at the pin support. The applied vertical load was captured by a
164 load cell (Item 2 in Fig. 5a) installed beneath the hydraulic jack. Meanwhile, two load cells (Item 7 in
165 Fig. 5a) were installed at jacking end of the strands to monitor the variation of prestressing forces
166 during tests. As shown in Fig. 5b, the overall vertical deflection of the beam and lateral movements
167 of the side column were measured by a series of linear variable differential transformers (LVDTs).
168 Moreover, strain gauges were mounted onto the reinforcements symmetrically before casting.

169 **3. Test results**

170 Eight specimens were tested through pushdown loading regime. The critical test results, for
171 instance, the first peak load (FPL), ultimate load (UL), and the maximum horizontal compressive or
172 tensile forces were summarized in Table 4. Fig. 6 illustrates the relationship of applied load versus
173 middle joint displacement (MJD) of tested specimens. More detail description and discussion could
174 be found in following sections.

175 **3.1. Global behavior and failure modes**

176 ***Specimens with bolted top-seat angle connection***

177 TSE and TSI have identical dimensions and reinforcement details except different boundary
178 conditions. The axial compressive force ratio of 0.2 was applied at the side column. Compared to
179 TSE, TSI has overhanging beam beyond the side column. It can be observed from Fig. 6 that TSI and
180 TSE obtained UL of 12.1 kN and 11.6 kN at MJD of 100 mm and 60 mm, respectively. The applied
181 load began to decrease gradually until the end of test. The test results indicated the TCA resistance of
182 TSE and TSI is negligible, as the beam reinforcements were discontinuity and the top-seat angle
183 unable to provide sufficient tie-force.

184 The failure modes of TSE and TSI were shown in Figs. 7 and 8, respectively. The beam and
185 column almost detached completely at large deformation stage. For TSE, the failure was concentrated
186 at the beam ends and only a few thin flexural cracks observed at the beam and side column. For TSI,
187 it was quite similar to that of TSE except no crack formed at the side columns. This is because the
188 overhanging beam restricted the deformation of the side columns effectively. It is worth noting that
189 the top-seat angles experienced limited deformation.

190 *Specimens with unbonded post-tensioning connection*

191 UPE-0.4 has effective prestress of $0.4f_{pu}$ in unbonded strand and the axial compressive force
192 ratio of the side column is 0.2. The FPL of UPE-0.4 was measured to be 30 kN at an MJD of 45 mm,
193 whereas the UL was measured to be 73 kN when the MJD up to 540 mm. Finally, test was stopped
194 due to excessive horizontal deflection in the right-hand side column. Fig. 9 shows the failure mode of
195 UPE-0.4. As shown in the figure, the failure mode of UPE was quite different to that of TSE and TSI.
196 Concrete crushing occurred at the compressive toes of the PC beam rather than concrete spalling
197 occurred at the beam end. No cracks occurred along the beam whereas wide opening was found at
198 beam-column interface due to fixed-end rotation. Moreover, due to tensile force from strands and
199 axial compression at the side column, a typical large eccentric compressive failure was observed at
200 the right-hand side column, which resulted in extensive flexural cracks occurred at the inner side of
201 the column, but severe concrete crushing occurred at the outer side. However, the left-hand side
202 column experienced much milder damage, only several thin flexural cracks formed in the inner side.
203 The different failure mode of two side columns was because the damage always occurs in relatively
204 weak side first and then concentrated in this side in the latter loading steps.

205 UPI-0.4 has overhanging beam at both sides. For UPI-0.4, the FPL of 35 kN was measured at
206 an MJD of 29 mm. Thus, the FPL of UPI-0.4 was approximately 116.6 % of that of UPE-0.4. With
207 the increase of MJD, the opening at the beam-column interfaces became wider and wider. Meanwhile,
208 the concrete crushing in the compressive toes of the beam end became more severe. When the MJD
209 reached 631 mm, one wire of the bottom strand fractured, as a result, the applied load dropped from
210 150 kN to 142 kN. Afterwards, the applied load kept increasing until the end of test. The UL of UPI-

211 0.4 was 151 kN at an MJD of 652 mm, which was approximately 206.8 % of that of UPE-0.4. As
212 shown in Fig. 10, the failure mode of UPI-0.4 was quite different to that of UPE-0.4. Wide opening
213 was observed at the beam-middle column interface and complete detach was observed between the
214 beam and side column surfaces. Thus, the progressive collapse resistance was totally provided by two
215 unbonded strands in large deformation stage. Moreover, due to considerable horizontal stiffness
216 provided by overhanging beam, the damage of the side column of UPI-0.4 was less severe and only
217 thin flexural cracks occurred along the side columns.

218 UPI-0.65 has similar dimensions and reinforcement details as UPI-0.4 except higher
219 effective prestress of $0.65f_{pu}$ was applied. When the MJD reached 39 mm, the FPL of 44 kN was
220 measured, which was 125.7 % of that of UPI-0.4. Thus, the specimen with higher effective prestress
221 would obtain higher resistance at small deformation stage. When the MJD reached 542 mm, the UL
222 of 131 kN, which was 86.8 % of that of UPI-0.4, was measured. After that, fracture of the wires of
223 the strands was observed consecutively until both two unbonded strands fractured completely at an
224 MJD of 628 mm. As shown in Fig. 11, except the fracture of both strands, the failure mode of UPI-
225 0.65 was quite similar to that of UPI-0.4.

226 ***Specimens with hybrid connection***

227 TSUPE-0.4, TSUPI-0.4, and TSUPI-0.65 were, respectively, have the enhancement over UPE-
228 0.4, UPI-0.4, and UPI-0.65 through extra bolted top-seat angle installed at the beam-column interface.
229 The FPL and UL of TSUPE-0.4 were 49 kN and 83 kN at MJD of 80 mm and 522 mm, respectively,
230 which were 163.3 % and 113.7 % of that of UPE-0.4, respectively. Thus, the bolted top-seat angle
231 enhanced the load resistance effectively, especially for the FPL at relatively small deformation stage.
232 Fig. 12 shows the failure mode of TSUPE-0.4. As shown in the figure, severe concrete spalling
233 occurred at the beam end and cracks formed at the beam end and side column. Moreover, concrete
234 crushing was observed at outer sider of the side columns. In general, the failure mode of TSUPE-0.4
235 was almost a combination of that of TSE and UPE-0.4 except top-seat angles achieved larger
236 deformation.

237 Compared to TSUPE-0.4, TSUPI-0.4 has overhanging beam beyond the side column. When
238 MJD reached 95 mm, the FPL of 51 kN, which is about 145.7 % of that of UPI-0.4, was measured.
239 Similar to TSUPE-0.4, **severe flexural cracks** were observed at the beam ends when the MJD reached
240 250 mm (about one beam depth). With increasing MJD to 330 mm, flexural crack was first observed
241 in the left side column. Test was stopped when the displacement reached 600 mm with a UL of 181
242 kN, which was approximately 119.9 % of that of UPI-0.4. As shown in Fig. 13, in general, the failure
243 mode of TSUPI-0.4 was quite similar to that of TSUPE-0.4 except TSUPI-0.4 experienced much
244 milder damage in side columns.

245 With a higher effective prestress of $0.65f_{pu}$, TSUPI-0.65 obtained a higher FPL of 64 kN at an
246 MJD of 76 mm. The UL of 178 kN was measured at an MJD of 600 mm. When the MJD reached 290
247 mm, the flexural cracks were first observed in the left side column, which were earlier than that of
248 TSUPI-0.4. As shown in Fig. 14, in general, the failure mode of TSUPI-0.65 was quite similar to that
249 of TSUPI-0.4. It was noted that the top-seat angles of TSUPI-0.65 experienced larger deformation
250 than that of TSUPI-0.4.

251 **3.2. Horizontal reaction**

252 Fig. 15 shows the comparison of total horizontal reaction versus MJD curves of tested
253 specimens while Table 4 tabulated the maximum horizontal reaction force. As shown in the figure
254 and Table 4, the maximum horizontal compressive force in UPE-0.4, UPI-0.4, UPI-0.65, TSUPE-0.4,
255 TSUPI-0.4, and TSUPI-0.65 were -66 kN, -96 kN, -84 kN, -50 kN, -93 kN, and -113 kN, respectively.
256 Therefore, UPE and TSUPE obtained much lower horizontal compressive force compared to the
257 counterpart UPI and TSUPI specimens due to no overhanging beams providing additional constraints.
258 In addition, the maximum tensile force of UPE-0.4, UPI-0.4, UPI-0.65, TSUPE-0.4, TSUPI-0.4, and
259 TSUPI-0.65 were 139 kN, 323 kN, 321 kN, 146 kN, 380 kN, and 364 kN, respectively. Comparison
260 of the maximum horizontal tensile force shows that UPE and TSUPE only achieved half of the
261 maximum horizontal tensile force as that of UPI and TSUPI specimens.

262 Fig. 16 illustrates the decomposition of the contribution of horizontal reaction force of UPI-0.4
263 and UPE-0.4. As shown in Fig. 16a, for UPI-0.4, bottom pin provided the largest contribution for the
264 compressive force while the overhanging beam provide the largest portion of the tensile force. For
265 specimen UPE-0.4, as no overhanging beams beyond the side column, the bottom pin and column top
266 roller provide almost similar contribution in tensile force. However, similar to UPI-0.4, majority of
267 the compressive force was contributed by the pin beneath the side column.

268 3.3. Deflection

269 Fig. 17a illustrates the overall deflection of the beams of UPI-0.65. As plastic hinges did not
270 form at the beam ends during the test, the beam elements deformed straightly. In general, the beams
271 in the specimens with UPT connection deformed straightly. Fig. 17b shows the deformation shape of
272 TSUPI-0.65. Different to UPI-0.65, TSUPI-0.65 was deformed in double curvature manner, which
273 agreed well with the observations that flexural action was mobilized at the beam end to resisted load.
274 Similar phenomena were observed for other specimens with hybrid connections. Figs. 18a and b
275 show the lateral deflection of the left side column of TSUPE-0.4 and TSUPI-0.4, respectively. As
276 shown in the figure, the side columns were pushed outward (negative value) firstly due to
277 compressive axial force developed in the beams. In large deformation stage, they were pulled inward
278 (positive value) because considerable tensile force developed in the strands. The measured maximum
279 inward movement in TSUPE-0.4 and TSUPI-0.4 were 24.2 mm and 6.2 mm, respectively. Compared
280 to TSUPE-0.4, due to desirable horizontal constraint provided by overhanging beams, the side
281 column of TSUPI-0.4 experienced less lateral deflection. In general, all the exterior side columns
282 (without overhanging beam) suffered a much larger deformation than interior ones (with overhanging
283 beam).

284 3.4. Strain gauge results

285 The strain distributions along beam longitudinal reinforcements of UPE-0.4, UPI-0.4, and
286 TSUPI-0.4 were demonstrated in Figs. 19, 20, and 21, respectively. As shown in the figure,
287 compressive strain about $-180 \mu\epsilon$ was initially measured due to the effects of effective prestress of

288 $0.4f_{pu}$ in post-tensioning strands. As shown in Fig. 19a, the strain of the bottom reinforcement near
289 the middle joint reduced to $0 \mu\epsilon$ when an MJD reached 20 mm, which could be explained as the
290 opening formed in the bottom of the beam end near the middle column. However, the strain of the
291 bottom reinforcement near the side column kept increasing with further increasing the MJD due to
292 the rotation of the beam end near the side column compacted the bottom of the beam section more
293 tightly. Conversely, due to similar reasons, for top reinforcements, the beam reinforcement near the
294 middle joint kept increasing with increase of the MJD while the beam reinforcement near the side
295 column decreased to $0 \mu\epsilon$ soon. As shown in Fig. 20, the varying of strain in beam longitudinal
296 reinforcement of UPI-0.4 was very similar to that of UPE-0.4. However, as illustrated in Fig. 21, the
297 strain gauge results in beam longitudinal reinforcements of TSUPI-0.4 were quite different. As
298 shown in Fig. 21a, for bottom reinforcements, tensile strain was measured at the beam end near the
299 middle joint when the MJD less than 250 mm. After MJD beyond 250 mm, the tensile strain began to
300 decrease as the top-seat angle began to quit work and wide opening occurred at the beam-middle
301 column interface. For the strain in the bottom reinforcement near the side column, compressive strain
302 of $-2281 \mu\epsilon$ was measured at an MJD of 100 mm. After that, the compressive strain began to decrease
303 as severe concrete crushing in the beam end. For the top reinforcement, the overall trend was similar
304 to that of the bottom rebar, whereas the maximum tensile and compressive strain, respectively, was
305 measured to be $1886 \mu\epsilon$ and $-2278 \mu\epsilon$ when the displacement up to 100 mm.

306 **3.5. Prestressing forces**

307 Fig. 22 shows the variation of total prestressing forces in unbonded strands. The initial effective
308 prestressing force in UPE-0.4, TSUPE-0.4, UPI-0.4, TSUPI-0.4, UPI-0.65, and TSUPI-0.65 were 153
309 kN, 148 kN, 150 kN, 146 kN, 237 kN, and 242 kN, respectively. In addition, the measured maximum
310 prestressing force in UPE-0.4, TSUPE-0.4, UPI-0.4, TSUPI-0.4, UPI-0.65, and TSUPI-0.65 were 269
311 kN, 277 kN, 323 kN, 364 kN, 329 kN, and 368 kN, respectively. Therefore, all the strands in the
312 specimens with overhanging beam reached their yield strength, which indicates the stronger
313 boundary better explores the full capacity of the prestress strands. Furthermore, it was found that the

314 prestressing forces in specimens with hybrid connections developed faster than others. This is
315 because, for a given MJD, the elongation of strands in these specimens was larger than others. It
316 should be noted that the strands in UPI series specimens fractured earlier than that in TSUPI series
317 specimens. This maybe because UPI series specimens concentrated the main rotation at the beam-
318 column interfaces (opening) whereas TSUPI series specimens deformed in a double-curvature
319 manner and the most critical section was at the edge of the top-seat angle plate, which resulted in the
320 stress distribution in the strands of TSUPI series more uniform.

321 **4. Discussions of the test results**

322 *4.1. Effects of boundary conditions*

323 As listed in Table 4, the FPL of UPE-0.4 and UPI-0.4 were 30 kN and 35 kN, respectively. In
324 addition, the UL of UPE-0.4 and UPI-0.4 were measured to be 73 kN and 151 kN, respectively.
325 Therefore, for specimens with UPT connections, stronger horizontal restraints could enhance the FPL
326 and UL by 16.7 % and 106.8 %, respectively. Furthermore, compared to UPI-0.4, UPE-0.4 achieved
327 less tensile force in strands, which could be explained to the large eccentric compression failure in
328 the side columns without overhanging beams. Regarding the failure modes, due to the additional
329 horizontal constraints of overhanging beam, the side columns of UPI-0.4 experienced much milder
330 damage, compared to UPE-0.4. For specimens with hybrid connection, the FPL of TSUPE-0.4 and
331 TSUPI-0.4 were 49 kN and 51 kN, respectively. Thus, the overhanging beams had little effects on the
332 PFL of the specimens with hybrid connections. When the MJD up to 600 mm and 522 mm, the UL of
333 TSUPI-0.4 and TSUPE-0.4 were measured to be 181 kN and 83 kN, respectively. Thus, due to the
334 overhanging beams, the TSUPI-0.4 increased UL by 118.1%, compared to TSUPE-0.4.

335 *4.2. Effect of effective prestress force*

336 As listed in Table 4. The FPL of UPI-0.4, UPI-0.65, TSUPI-0.4, and TSUPI-0.65 were 35 kN, 44
337 kN, 51 kN, and 64 kN, respectively. Thus, the higher effective prestress in post-tensioning strands
338 could increase the FPL of UPI and TSUPI series by 25.7 % and 27.5 %, respectively. As shown in
339 Fig. 6, the growth of load resistance of UPI-0.65 and TSUPI-0.65 were slower than that of UPI-0.4

340 and TSUPI-0.4 at the beginning of the test. This is mainly due to the higher effective prestress force
341 may result in the strands reach their yield strength earlier. Moreover, the fracture of strand was firstly
342 observed in UPI-0.65 at an MJD of 542 mm while it was 621 mm for UPI-0.4. Thus, the higher
343 effective prestress may lead to earlier fracture of the strands and reduce its deformation capacity.
344 Therefore, in general, lower effective (less than $0.65 f_{pu}$) prestress was preferred for post-tensioned
345 precast concrete frame to resist progressive collapse, similar to Cheok and Lew [40] for seismic
346 resisting design.

347 **4.3. Effect of top-seat angle**

348 Compared to UPI-0.4, TSUPI-0.4 increased the FPL and UL by 45.7 % and 19.9 %, respectively.
349 Thus, installing top-seat angle could improve the collapse resistance effectively. Moreover, due to the
350 rotation restraint provided by the top-seat angle, the failure mode TSUPI-0.4 was significantly
351 different to that of UPI-0.4. For UPI-0.4, wide opening was observed at the beam-column interface
352 and no crack occurred along the beam. For TSUPI-0.4, severe flexural cracks were observed in the
353 beams. Similar results were observed in TSUPE-0.4 and TSUPI-0.65. In general, installing top-seat
354 angle could enhance the load resistance significantly and the flexural action could be mobilized to
355 resist progressive collapse.

356 Fig. 23a compares the load resistance of TSUPI-0.4 to the superposition of TSI and UPI-0.4.
357 As shown in the figure, the resistance of TSUPI-0.4 was larger than the superposition of TSI and
358 UPI-0.4 from the beginning to the end. Thus, the hybrid connection achieved better resistance than
359 the overall resistance capacity of two separate connections effect of one plus one over two. This is
360 because the top-seat angle evoked flexural action and reduced the effective length of beam. In
361 general, similar observations were obtained for TSUPE-0.4 and TSUPI-0.65, as shown in Fig. 23b
362 and c.

363 **4.4. Dynamic load resistance**

364 Based on the energy balance method proposed by Izzuddin [41], the external work is equal to
365 the strain energy increased in the remained structure. Thus, the quasi-static progressive collapse

366 resistance can be converted to dynamic resistance, that is, pseudo-static progressive collapse
367 resistance. The dynamic progressive resistance can be determined by equation below:

$$368 \quad P_{CC}(u_d) = \frac{1}{u_d} \int_0^{u_d} P_{NS}(u) du \quad (1)$$

369 where $P_{CC}(u)$ and $P_{NS}(u)$ represent the capacity function and the nonlinear static loading estimated
370 at the displacement demand u , respectively.

371 Fig. 24 illustrates the dynamic load resistance of the tested specimens. The dynamic load
372 resistance of UPE-0.4, UPI-0.4, UPI-0.65, TSUPE-0.4, TSUPI-0.4, and TSUPI-0.65 were 49 kN, 71
373 kN, 67 kN, 62 kN, 89 kN and 91 kN, respectively. As shown in the figure, installing top-seat angles
374 could enhance the dynamic load resistance up by 35.8 %.

375 **4.5. Load resisting mechanisms**

376 Typical load resisting mechanisms of conventional RC frame are demonstrated in Fig. 25. As
377 shown in Fig. 25a, flexural action and CAA were mobilized in sequence to resist progressive collapse
378 at relatively small deformation stage. Flexural action depends on the bending moment capacity of the
379 plastic hinge whereas CAA relies on the horizontal constraints at the beam ends. In general, with the
380 increase of the MJD, the concrete crushing may lead to the termination of CAA. When the MJD
381 exceeds about one beam depth, as shown in Fig. 25b, the axial force in the beam may change from
382 compression to tension and TCA was mobilized to resist load. For RC structures, the decreasing of
383 TCA was usually accompanied by rebar fracture. Moreover, penetrate cracks usually occur along the
384 beam due to tensile axial force.

385 However, the load resisting mechanisms developed in PC frames observed in this study were
386 quite different to that of conventional RC frames, as shown in Fig. 26. For specimens with UPT
387 connection, as no beam longitudinal rebar passed through the beam-column joint, plastic hinge would
388 not form at the beam end and thus, flexural action was not mobilized to resist the load. From the
389 beginning of the test, the CAA and the tensile force developed in the strands together to resist the
390 load. However, different to RC frames, the CAA mobilized in beam will not be terminated as the
391 compressive force was actively applied by prestressing strands. Thus, the CAA may have a negative

392 contribution to the load resistance when the displacement beyond about one beam depth. As shown in
393 Fig. 26a, when the displacement was small, the arching force (N in the figure) developed in beams
394 started to help to resist the vertical load (P in the figure). However, when the displacement exceeded
395 about one beam depth, as shown in Fig. 26b, the direction of resultant force of the arching force
396 would change from upward to downward, and thus, negative contribution generated. For specimens
397 with UPT connections, as the CAA and TCA provided the load resistance independently. The
398 contribution from TCA could be determined by the vertical component of prestressing forces. The
399 contribution from CAA can be simply determined by subtracting the resistance of TCA from the
400 measured load resistance. For the sake of brevity, only the decomposition of load resisting capacity
401 of UPI-0.65 was shown in Fig. 27. As shown in the figure, the contribution of load resistance from
402 TCA was always positive while the contribution of CAA will change from positive to negative when
403 the vertical displacement beyond about one beam depth.

404 As shown in Fig. 28, for specimen with hybrid connection, flexural action was mobilized to
405 resist progressive collapse as the top-seat angle constraints the rotation of beam end. It should be
406 noted that, as the flexural action could not be simply determined. The decomposition of load
407 resistance of specimens with hybrid connection was not shown herein. More detailed analysis should
408 be carried out to determine the flexural action in the specimens with hybrid connection in the future
409 study.

410 **5. Conclusions**

411 Based on the experimental results, the following conclusions can be drawn:

- 412 1. In RC structure, tensile catenary action (TCA) is kicked in after compressive arch action (CAA).
413 However, in current study, the TCA in unbonded post-tensioning strands can be mobilized at the
414 beginning of the test. Thus, the CAA and TCA can work simultaneously.
- 415 2. Different to RC frame, as no beam longitudinal reinforcements pass through the beam-column
416 joint and the strands are unbonded, flexural action would not be developed to resist progressive
417 collapse for the specimens with unbonded post-tensioning connection. However, flexural action

- 418 can develop in specimens with top-seat angle due to the top-seat angle constrains the rotation of
419 beam end partially.
- 420 3. For conventional RC frame, CAA will be terminated when the vertical displacement beyond
421 about one beam depth due to concrete crushing. However, in this study, the CAA developed in
422 PC frames with unbonded post-tensioning strands was mainly due to prestressing force of the
423 strands and thus, the CAA will not vanish until the beam and column separate completely
424 (prestressing force will not generate compressive stress in the beam concrete). The CAA even
425 generates negative contribution to load resistance when the vertical displacement exceeds about
426 one beam depth.
- 427 4. Installing top-seat angle could improve the behavior by evoking flexural action and reducing the
428 effective length of beam. On the other hand, the top-seat angle may lead to more severe damage
429 in beam, especially in the beam end, resulting in less reparability of frame.
- 430 5. Higher effective prestress benefits the development of the resistance at small deformation.
431 However, the higher effective prestress may reduce the deformation capacity of the strands,
432 leading to the earlier strand fracture and lower ultimate load capacity.
- 433 6. Stronger boundary condition could improve the performance of the frame in terms of load
434 resistance and deformation capacity. The failure of the specimens without overhanging beams
435 was controlled by the large eccentric compression failure at the side columns. However, the
436 failure of specimens with overhanging beams was controlled by the fracture of strands. Thus, the
437 specimens have overhanging beam could fully use the material properties of the strands.

438 **6. Acknowledgements**

439 This research was supported by a research grant provided by the Natural Science Foundation of
440 China (Nos. 51568004, 51778153, 51868004). Any opinions, findings and conclusions expressed in
441 this paper are those of the writers and do not necessarily reflect the view of Natural Science
442 Foundation of China.

443

444

445 **References**

- 446 [1] Su YP, Tian Y, Song XS. Progressive collapse resistance of axially-restrained frame beams. *ACI*
447 *Structural Journal* 2009; 106(5): 600-607.
- 448 [2] Sadek F, Main J, Lew H, Bao Y. Testing and analysis of steel and concrete beam-column
449 assemblies under a column removal scenario. *Journal of Structural Engineering* 2011; 137(9):
450 881-892.
- 451 [3] Yu J, Tan KH. Experimental and numerical investigation on progressive collapse resistance of
452 reinforced concrete beam column sub-assemblages. *Engineering Structures* 2013; 55: 90-106.
- 453 [4] Yu J, Tan KH. Special detailing techniques to improve structural resistance against progressive
454 collapse. *Journal of Structural Engineering* 2014; 140(3): 04013077.
- 455 [5] Ren PQ, Li Y, Lu XZ, Guan H, Zhou YL. Experimental investigation of progressive collapse
456 resistance of one-way reinforced concrete beam-slab substructures under a middle-column-
457 removal scenario. *Engineering Structures* 2016; 118: 28-40.
- 458 [6] Lu XZ, Lin KQ, Li Y, Guan H, Ren PQ, Zhou YL. Experimental investigation of RC beam-slab
459 substructures against progressive collapse subject to an edge-column-removal scenario.
460 *Engineering Structures* 2017; 149: 91-103.
- 461 [7] Qian K, Li B, Ma JX. Load-carrying mechanism to resist progressive collapse of RC buildings.
462 *Journal of Structural Engineering* 2015; 141(2): 04014107
- 463 [8] Qian K, Li B. Performance of Three-dimensional reinforced concrete beam-column substructures
464 under loss of a corner column scenario. *Journal of Structural Engineering* 2013; 139(4): 584-594.
- 465 [9] Qian K, Li B. Dynamic performance of RC beam-column substructures under the scenario of the
466 loss of a corner column—Experimental results. *Engineering Structures* 2012; 42: 154-167.
- 467 [10] Qian K, Li B. Slab effects on response of reinforced concrete substructures after loss of corner
468 column. *ACI structural Journal* 2012; 109: 845-855.
- 469 [11] Qian K, Li B. Quantification of slab influences on the dynamic performance of RC frames
470 against progressive collapse. *J. Perform. Constr. Facil* 2015; 29(1): 04014029.
- 471 [12] Shan SD, Li S, Xu SY, Xie LL. Experimental study on the progressive collapse performance of
472 RC frames with infill walls. *Engineering Structures* 2016; 111: 80-92.
- 473 [13] Peng ZH, Orton SL, Liu JR, Tian Y. Experimental study of dynamic progressive collapse in flat-
474 plate buildings subjected to exterior column removal. *Journal of Structural Engineering* 2017;
475 143(9): 04017125.
- 476 [14] Peng ZH, Orton SL, Liu JR, Tian Y. Experimental study of dynamic progressive collapse in flat-
477 plate buildings subjected to interior column removal. *Journal of Structural Engineering* 2018;
478 144(8): 04018094.

- 479 [15] Ma F, Gilbert B, Guan H, Xue HZ, Lu XZ, Li Y. Experimental study on the progressive collapse
480 behaviour of RC flat plate substructures subjected to corner column removal scenarios.
481 Engineering Structures 2019; 180: 728-741.
- 482 [16] Qian K, Weng YH, Li B. Improving behavior of reinforced concrete frames to resist progressive
483 collapse through steel bracings. Journal of Structural Engineering 2019; 145(2): 04018248.
- 484 [17] Sasani M, Bazan M, Sagioglu S. Experimental and analytical progressive collapse evaluation of
485 actual reinforced concrete structure. ACI Structural Journal 2007; 104(6): 731-9.
- 486 [18] Sasani M, Sagioglu S. Progressive collapse resistance of Hotel San Diego. Journal of Structural
487 Engineering 2008; 134(3): 478-88.
- 488 [19] Sasani M. Response of a reinforced concrete infilled-frame structure to removal of two adjacent
489 columns. Engineering Structures 2008; 30: 2478-91.
- 490 [20] Sasani M, Sagioglu S. Gravity load redistribution and progressive collapse resistance of 20-
491 story reinforced concrete structure following loss of interior column. ACI Structural Journal
492 2010; 107(6): 636-44.
- 493 [21] Sasani M, Kazemi A, Sagioglu S, Forest S. Progressive collapse resistance of an actual 11-story
494 structure subjected to severe initial damage. Journal of Structural Engineering 2011; 137(9): 893-
495 902.
- 496 [22] Nimse RB, Joshi DD, Oatel PV. Behavior of wet precast beam column connections under
497 progressive collapse scenario: an experimental study. International Journal of Advanced
498 Structural Engineering 2014; 6: 149-159.
- 499 [23] Kang SB, Tan KH. Behaviour of precast concrete beam-column sub-assemblages subject to
500 column removal. Engineering Structures 2015; 93: 85-96.
- 501 [24] Kang SB, Tan KH. Robustness assessment of exterior precast concrete frames under column
502 removal scenarios. Journal of Structural Engineering 2016; 142(12): 04016131.
- 503 [25] Keyvani L. Progressive collapse resistance of reinforced and post-tensioned flat plate structures.
504 PhD Dissertation, The Department of Civil and Environmental Engineering, Northeastern
505 University; 2015.
- 506 [26] Keyvani L, Sasani M. Analytical and experimental evaluation of progressive collapse resistance
507 of a flat-slab posttensioned parking garage. Journal of Structural Engineering 2015; 141(11):
508 04015030.
- 509 [27] Qian K, Li B. Investigation into resilience of precast concrete floors against progressive collapse.
510 ACI Structural Journal 2019; 116(2): 171-182.
- 511 [28] Al-Salloum YA, Alrubaidi MA, Elsanadedy HM, Almusallam TH, Iqbal RA. Strengthening of
512 precast RC beam-column connections for progressive collapse mitigation using bolted steel
513 plates. Engineering Structures 2018; 161: 146-160.

- 514 [29] Quiel SE, Naito CJ, Fallon CT. A non-emulative moment connection for progressive collapse
515 resistance in precast concrete building frames. *Engineering Structures* 2019; 179: 174-188.
- 516 [30] Qian K, Li B. Performance of precast concrete substructures with dry connections to resist
517 progressive collapse. *Journal of Performance of Constructed Facilities* 2018; 32(2): 04018005.
- 518 [31] Priestley MJN, MacRae G. Seismic tests of precast beam-to-column joint subassemblages with
519 unbonded strands. *PCI J* 1996; 41(1): 64-81.
- 520 [32] Cheok G, Lew H. Model precast concrete beam-to-column joints subject to cyclic loading. *PCI J*
521 1993; 38(4): 80-92.
- 522 [33] Stone WC, Cheok GS, Stanton JF. Performance of hybrid moment-resisting precast beam-
523 column concrete connection subjected to cyclic loading. *ACI Structural Journal* 1995; 92(2):
524 229-49.
- 525 [34] Stanton J, Stone WC, and Cheok GS. A Hybrid Reinforced Precast Frame for Seismic Regions.
526 *PCI Journal* 1997, 42(2): 20-32.
- 527 [35] Rodgers GW, Solberg KM, Chase JG, Mander JB, Bradley BA, Dhakal RP, Li L. Performance
528 of a damage-protected beam-column subassembly utilizing external HF2V energy dissipation
529 devices. *Earthquake Engineering and Structural Dynamics* 2008; 37(13): 1549–64.
- 530 [36] Rodgers GW, Solberg KM, Mander JB, Chase JG, Bradley BA, Dhakal RP. Highforce-to-
531 volume seismic dissipaters embedded in a jointed precast concrete frame. *Journal of Structural*
532 *Engineering* 2012; 138(3): 375–86.
- 533 [37] Song LL, Guo T, Chen C. Experimental and numerical study of a self-centering prestressed
534 concrete moment resisting frame connection with bolted web friction devices. *Earthquake*
535 *Engineering and Structural Dynamics* 2014; 43(4): 529–45.
- 536 [38] Song LL, Guo T, Gu Y, Cao ZL. Experimental study of a self-centering prestressed concrete
537 frame subassembly. *Engineering Structures* 2015; 88: 176-188.
- 538 [39] **ACI Committee 318, Building Code Requirements for Structural Concrete (ACI 318-14) and**
539 **Commentary (318R-14). American Concrete Institute, Farmington Hills, MI, 433 pp; 2014.**
- 540 [40] **Cheok GS and Lew HS. Performance of precast concrete beam-to-column connections subject**
541 **to cyclic loading. PCI Journal 1991, 36(3): pp. 56-67.**
- 542 [41] Izzuddin B, Vlassis A, Elghazouli A, Nethercot D. Progressive collapse of multi-storey
543 buildings due to sudden column loss-part I: simplified assessment framework. *Engineering*
544 *Structures* 2008; 30: 1308-1318.
- 545
- 546
- 547
- 548

549 **Figure caption list**

550 **Fig. 1.** Bending moment diagram of a frame: (a) before removal of column; (b) after removal of
551 column

552 **Fig. 2.** Tested connections: (a) unbonded post-tensioning connection; (b) hybrid connection; (c)
553 bolted top-seat angle connection

554 **Fig. 3.** Details of test specimens: (a) TSUPI; (b) UPE; (c) cross sections

555 **Fig. 4.** Stress-strain constitutive curves: (a) rebar; (b) post-tensioning strands

556 **Fig. 5.** Test setup and instrumentation: (a) photo; (b) elevation view

557 **Fig. 6.** Vertical load-displacement curves

558 **Fig. 7.** Failure mode of TSE

559 **Fig. 8.** Failure mode of TSI

560 **Fig. 9.** Failure mode of UPE-0.4

561 **Fig. 10.** Failure mode of UPI-0.4

562 **Fig. 11.** Failure mode of UPI-0.65

563 **Fig. 12.** Failure mode of TSUPE-0.4

564 **Fig. 13.** Failure mode of TSUPI-0.4

565 **Fig. 14.** Failure mode of TSUPI-0.65

566 **Fig. 15.** Comparison of the horizontal reaction force versus MJD curves

567 **Fig. 16.** Contribution of horizontal reaction force from each constraint: (a) UPI-0.4; (b) UPE-0.4

568 **Fig. 17.** Overall deflection of double-bay beam: (a) UPI-0.65; (b) TSUPI-0.65

569 **Fig. 18.** Horizontal deformation in side column: (a) TSUPE-0.4; (b) TSUPI-0.4

570 **Fig. 19.** Strain distribution in beam longitudinal reinforcement of UPE-0.4: (a) bottom rebar; (b) top
571 rebar

572 **Fig. 20.** Strain distribution in beam longitudinal reinforcement of UPI-0.4: (a) bottom rebar; (b) top
573 rebar

574 **Fig. 21.** Strain distribution in beam longitudinal reinforcement of TSUPI-0.4: (a) bottom rebar; (b)
575 top rebar

576 **Fig. 22.** Total prestressing forces-displacement relationship

577 **Fig. 23.** Discussion of each design variable: (a) TSUPI-0.4; (b) TSUPE-0.4; (c) TSUPI-0.65

578 **Fig. 24.** Dynamic resistance of tested specimens

579 **Fig. 25.** Load resisting mechanism of RC structure: (a) compressive arch action; (b) tensile catenary

580 action

581 **Fig. 26.** Load resisting mechanisms of specimens with unbonded post-tensioning connection: (a)

582 small deformation; (b) MJD beyond one beam depth

583 **Fig. 27.** Resistance decomposition of specimen UPI-0.65

584 **Fig. 28** Load resisting mechanism of specimens with hybrid connection

585

586

587

588

589

590

591

592

593

594

595

596

597

598

599

600

601

602

603

604

605

606

607

608

609

610

611

612

613

614

615

616

617

618

619

620
621
622

Table 1. Relationship between prototype frames and corresponding test specimens

Test ID	Prototype frame			Test specimen		
	Column (mm × mm)	Beam (mm × mm)	Diameter of strands (mm)	Column (mm × mm)	Beam (mm × mm)	Diameter of strands (mm)
TSE	500×500	500×300	N/A	250×250	250×150	N/A
TSI	500×500	500×300	N/A	250×250	250×150	N/A
UPE-0.4	500×500	500×300	4×17.8	250×250	250×150	2×12.7
UPE-0.65	500×500	500×300	4×17.8	250×250	250×150	2×12.7
UPI-0.4	500×500	500×300	4×17.8	250×250	250×150	2×12.7
UPI-0.65	500×500	500×300	4×17.8	250×250	250×150	2×12.7
TSUPI-0.4	500×500	500×300	4×17.8	250×250	250×150	2×12.7
TSUPI-0.65	500×500	500×300	4×17.8	250×250	250×150	2×12.7

623
624
625
626
627

Table 2. Specimens properties

Test ID	Span/depth ratio	Axial compression ratio	Top (Bottom) beam rebar ratio ρ	Column rebar ratio ρ	Effective prestress	Top-seat angle	Overhanging beam
TSE	12	0.2	0.6% (0.6%)	1.4%	N/A	L160×12	N/A
TSI	12	0.2	0.6% (0.6%)	1.4%	N/A	L160×12	Yes
UPE-0.4	12	0.2	0.6% (0.6%)	1.4%	$0.4f_{pu}$	N/A	N/A
UPI-0.4	12	0.2	0.6% (0.6%)	1.4%	$0.4f_{pu}$	N/A	Yes
UPI-0.65	12	0.2	0.6% (0.6%)	1.4%	$0.65f_{pu}$	N/A	Yes
TSUPE-0.4	12	0.2	0.6% (0.6%)	1.4%	$0.4f_{pu}$	L160×12	N/A
TSUPI-0.4	12	0.2	0.6% (0.6%)	1.4%	$0.4f_{pu}$	L160×12	Yes
TSUPI-0.65	12	0.2	0.6% (0.6%)	1.4%	$0.65f_{pu}$	L160×12	Yes

628
629
630
631
632
633
634

Note: f_{pu} is the nominal ultimate strength of the post-tensioning strands (1860 MPa); rebar ratio is determined using equation $\rho = A_s/bd_0$, in which A_s , b and d_0 represent the area of rebar, width and the effective depth of beam cross sections, respectively.

Table 3. Material properties

Item	Nominal diameter (mm)	Yield strength (MPa)	Ultimate strength (MPa)	Elastic modulus (MPa)	Elongation (%)
Transverse reinforcements R6	6	368	485	162,000	20.1
Longitudinal reinforcements T12	12	462	596	171,000	14.7
Longitudinal reinforcements T16	16	466	604	182,000	17.0
Posttensioning strands	12.7	1,649	1,970	213,000	6.3

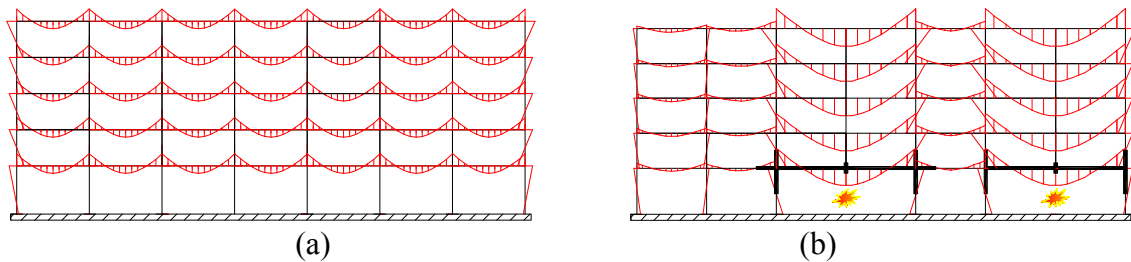
635
636
637
638
639
640
641
642

643
644
645
646

Table 4. Summary of test results

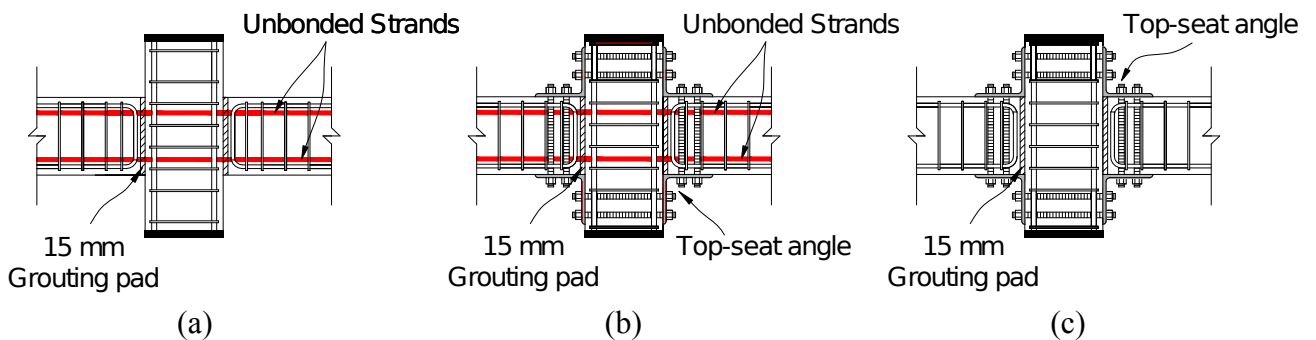
Specimen identifier	Critical displacement (mm)		Critical load (kN)		Maximum prestressing force (kN)	Maximum horizontal compressive/tensile force (kN)
	First peak load	Ultimate load	First peak load	Ultimate load		
TSE	70	70	12	12	N/A	-37/18
TSI	100	100	12	12	N/A	-44/3
UPE-0.4	45	540	30	73	269	-66/139
UPI-0.4	29	652	35	151	324	-96/323
UPI-0.65	39	542	44	131	326	-84/321
TSUPE-0.4	100	522	49	83	277	-50/146
TSUPI-0.4	95	600	51	181	364	-93/380
TSUPI-0.65	76	600	64	178	368	-113/364

647
648
649
650



651
652
653
654
655
656

Fig. 1. Bending moment diagram of a frame: (a) before removal of column; (b) after removal of column

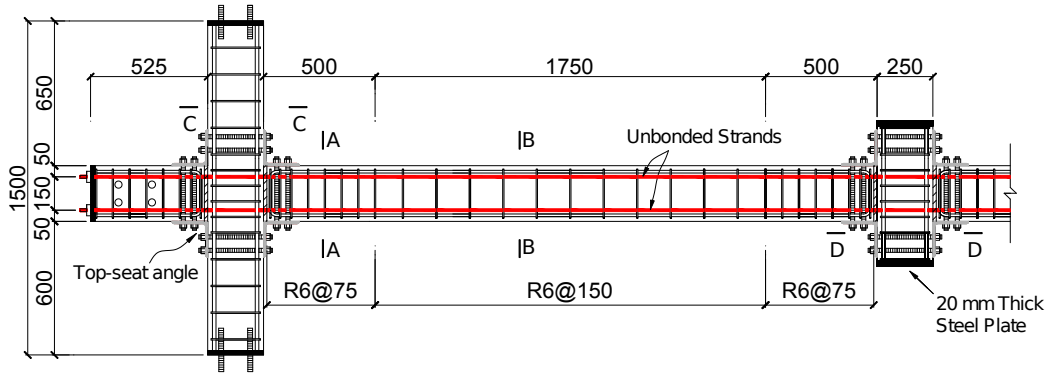


657
658

Fig. 2. Test connections: (a) unbonded post-tensioning connection; (b) hybrid connection; (c) bolted top-seat angle connection

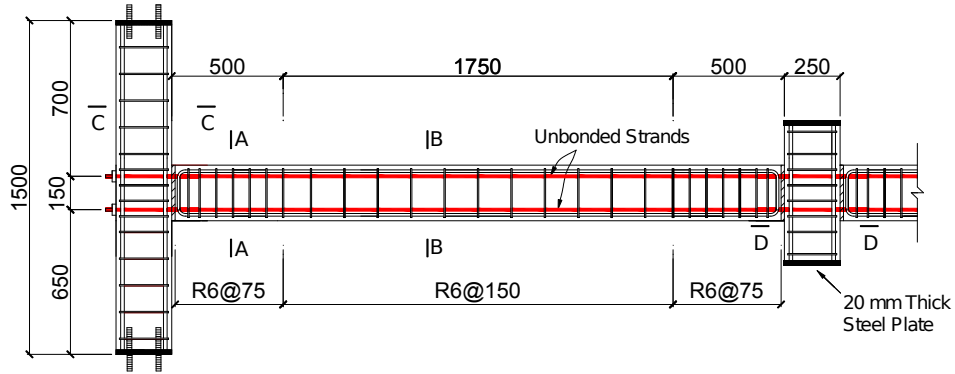
660
661
662
663
664
665
666
667
668
669

670
671



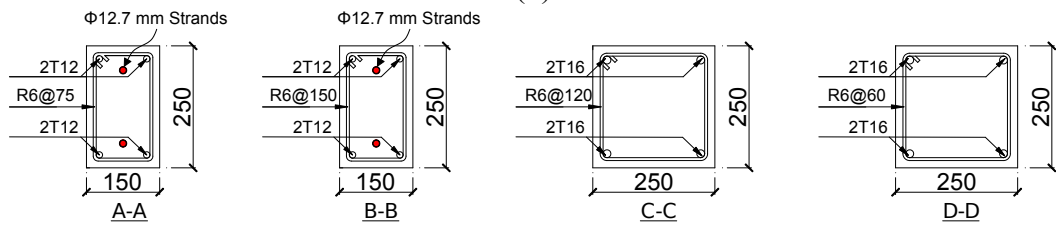
672
673

(a)



674
675

(b)



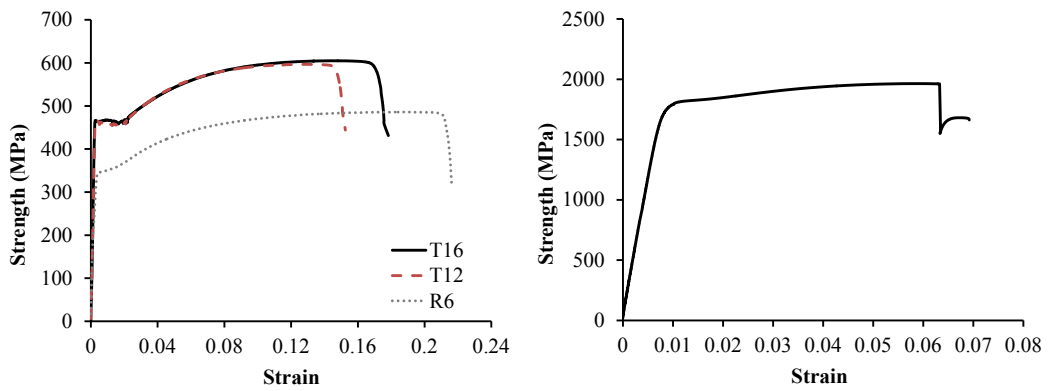
676
677

(c)

678
679

Fig. 3. Details of test specimens: (a) TSUPI; (b) UPE; (c) cross sections

680
681
682
683



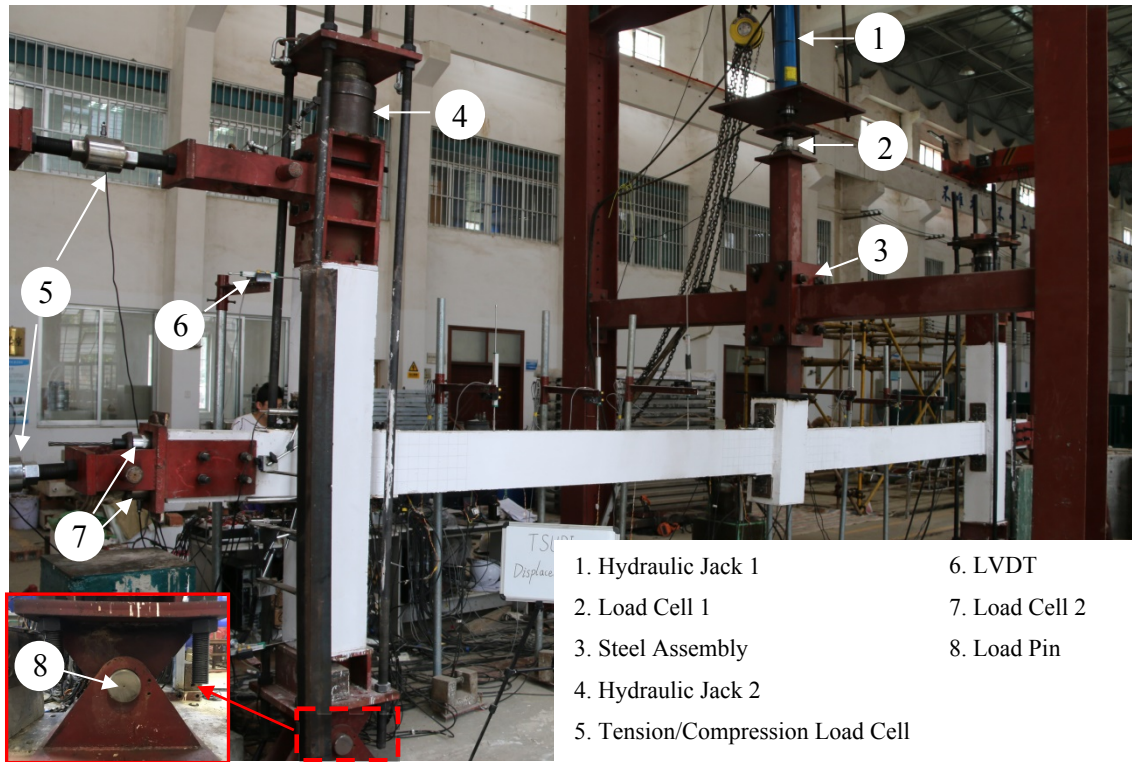
684
685
686
687
688
689

(a)

(b)

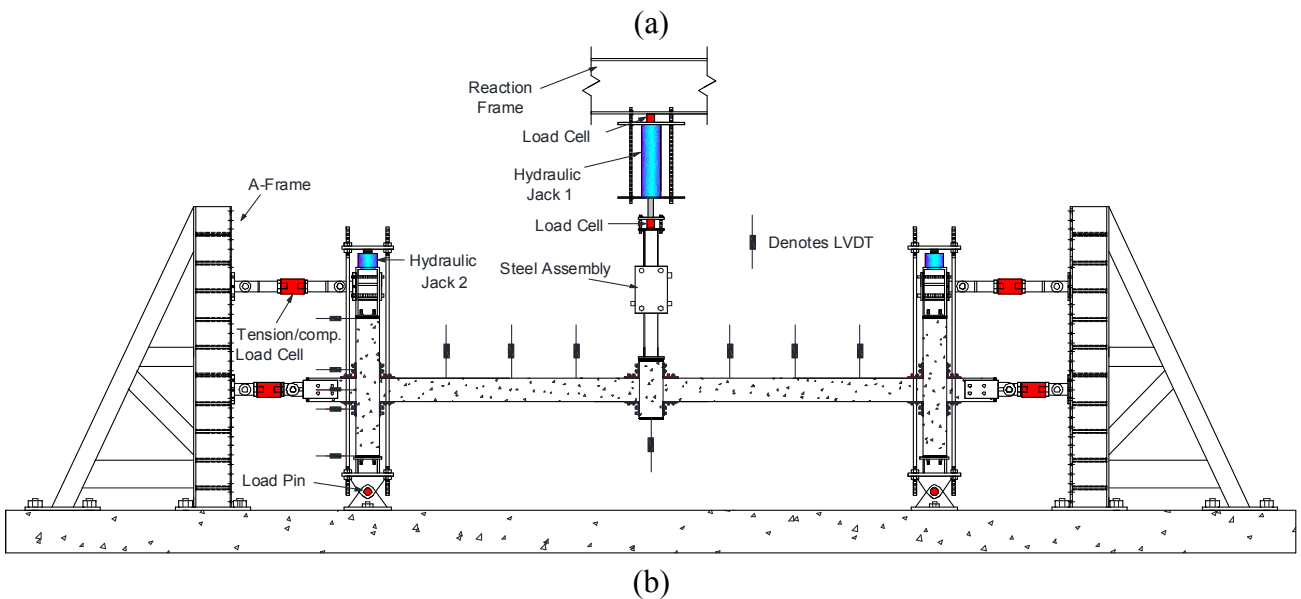
Fig. 4. Stress-strain constitutive curves: (a) rebar; (b) post-tensioning strands

690
691
692



- 1. Hydraulic Jack 1
- 2. Load Cell 1
- 3. Steel Assembly
- 4. Hydraulic Jack 2
- 5. Tension/Compression Load Cell
- 6. LVDT
- 7. Load Cell 2
- 8. Load Pin

693
694



695
696
697
698
699
700
701

Fig. 5. Test setup and instrumentation: (a) photo; (b) elevation view

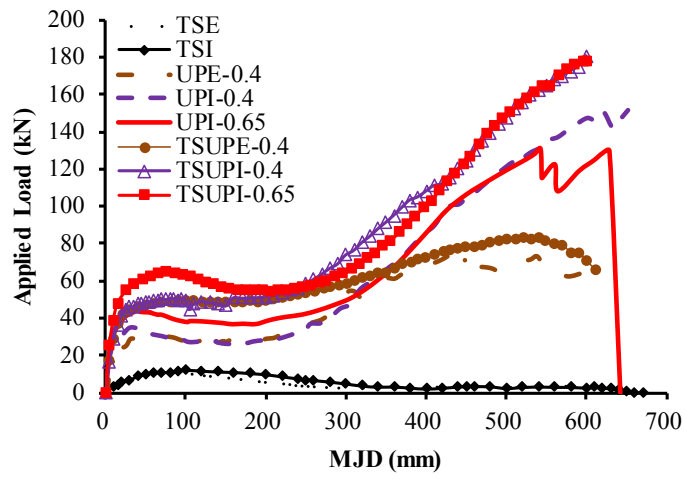


Fig. 6. Vertical load-displacement curves

702
703
704
705
706
707

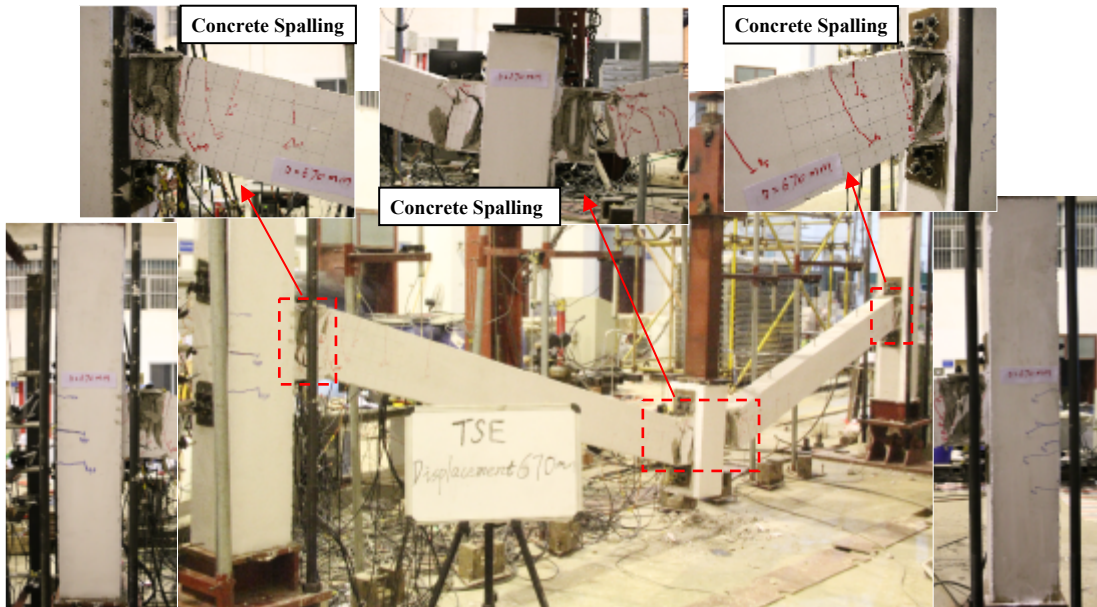


Fig. 7. Failure mode of TSE

708
709
710
711
712
713
714
715
716
717
718
719
720
721
722
723
724
725
726

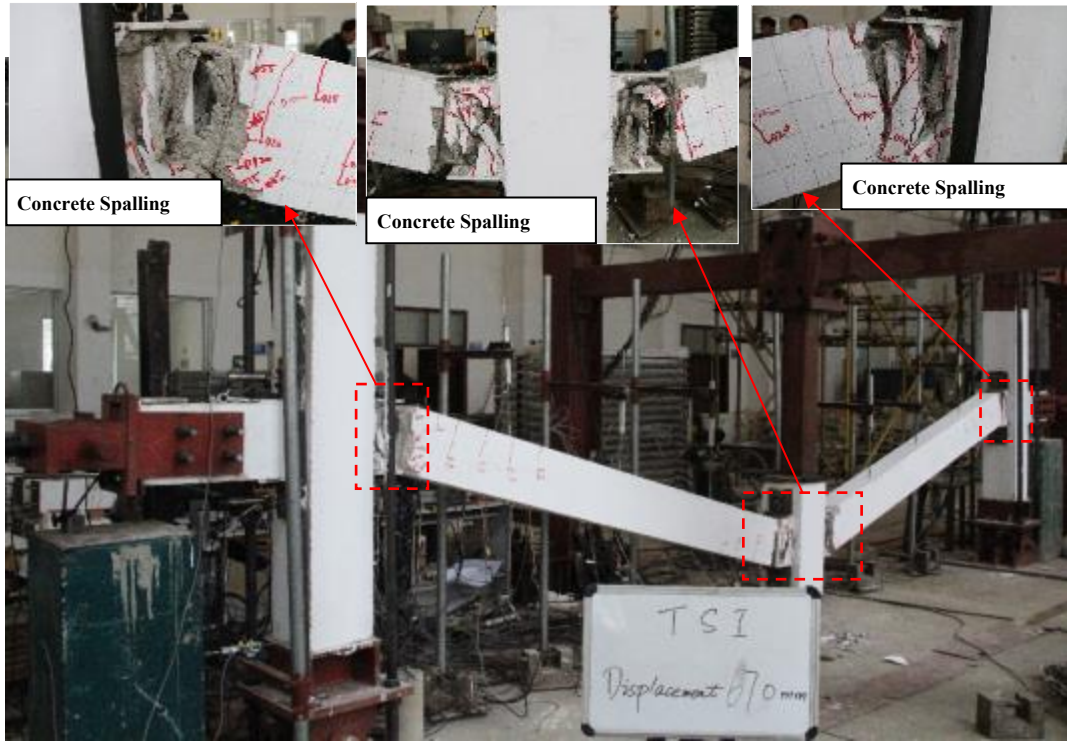


Fig. 8. Failure mode of TSI

727
728
729
730
731

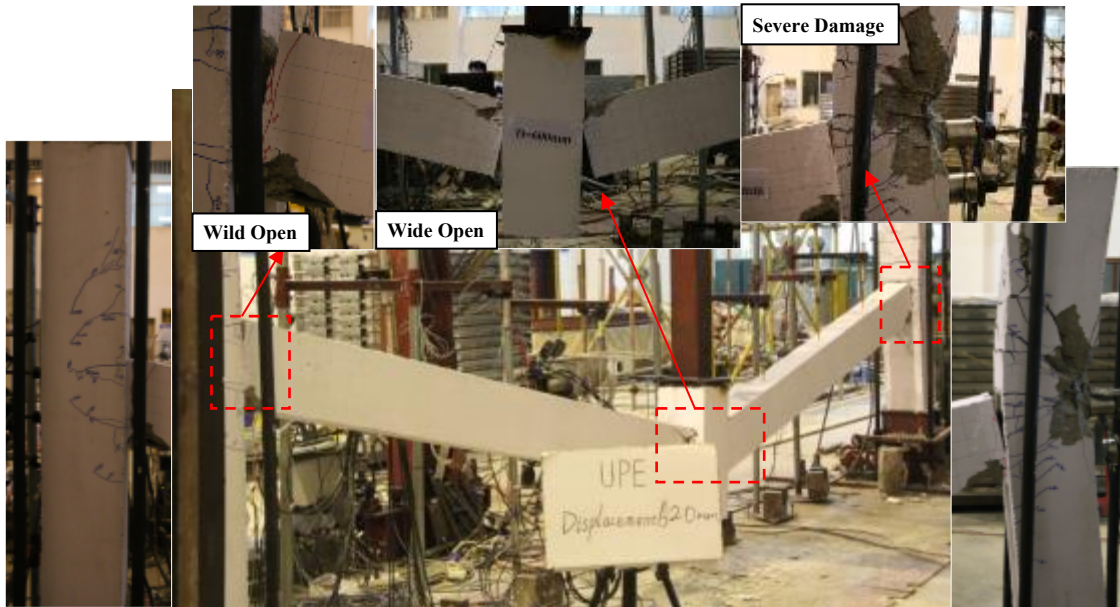


Fig. 9. Failure mode of UPE-0.4

732
733
734
735
736
737
738
739
740
741
742
743
744
745

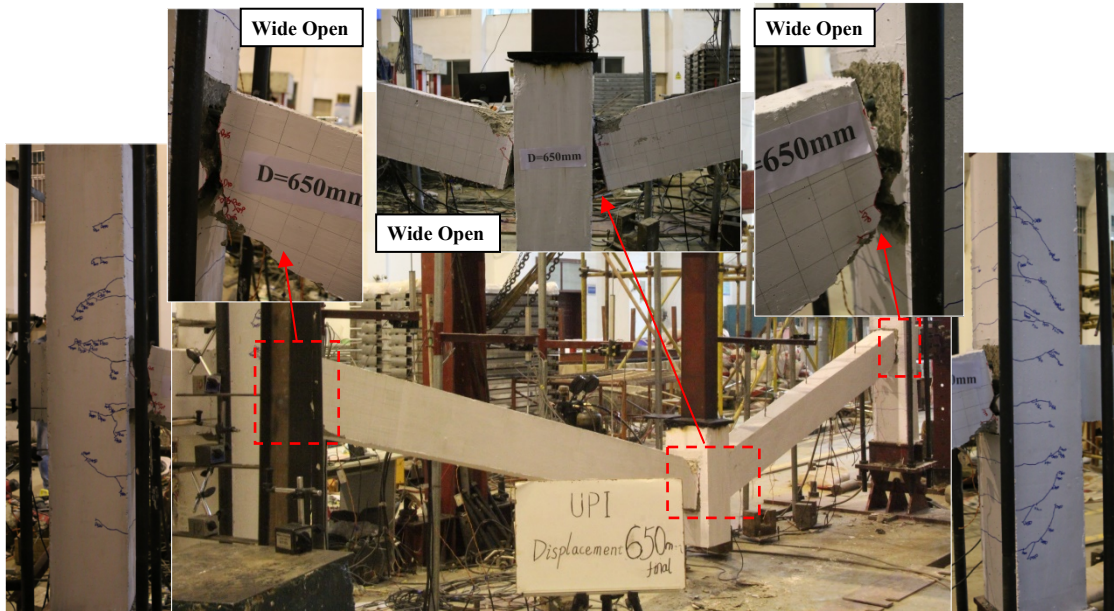


Fig. 10. Failure mode of UPI-0.4

746
747
748
749
750
751

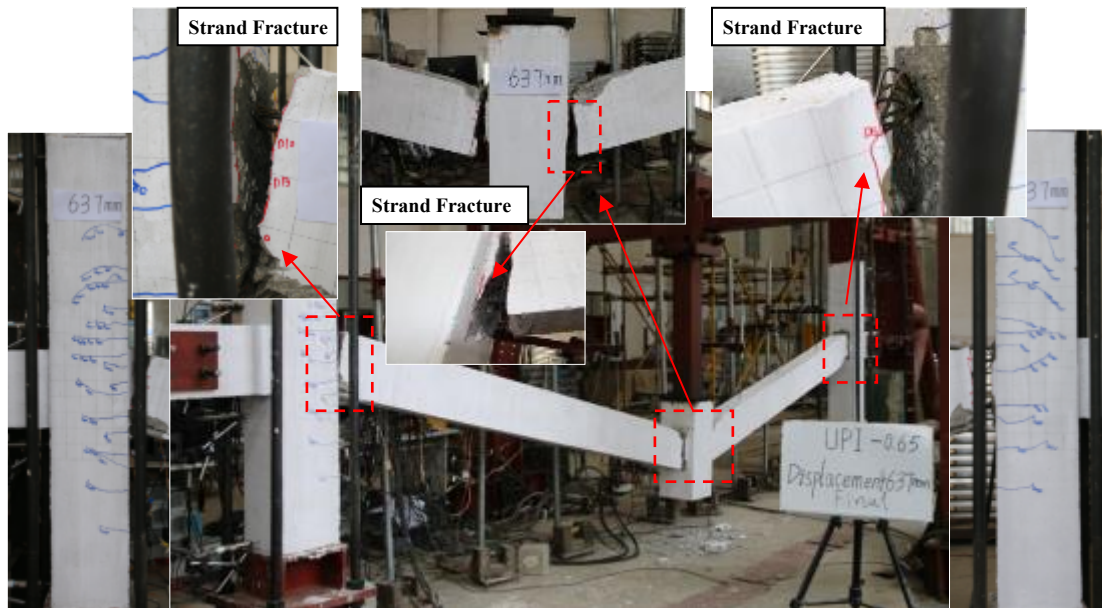


Fig. 11. Failure mode of UPI-0.65

752
753
754
755
756
757
758
759
760
761
762
763
764
765
766
767

768
769
770

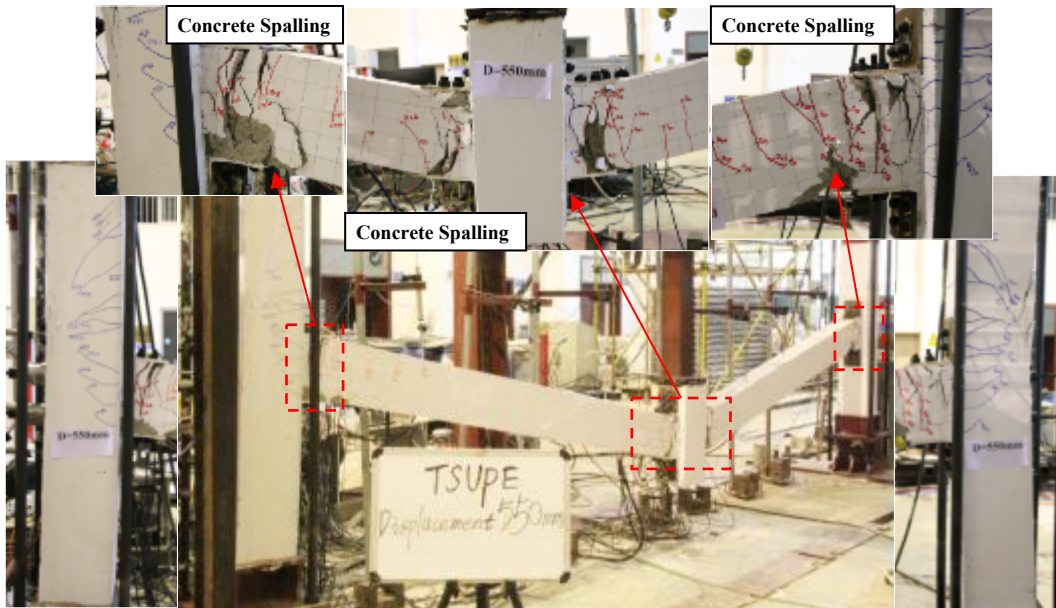


Fig. 12. Failure mode of TSUPE-0.4

771
772
773
774
775
776

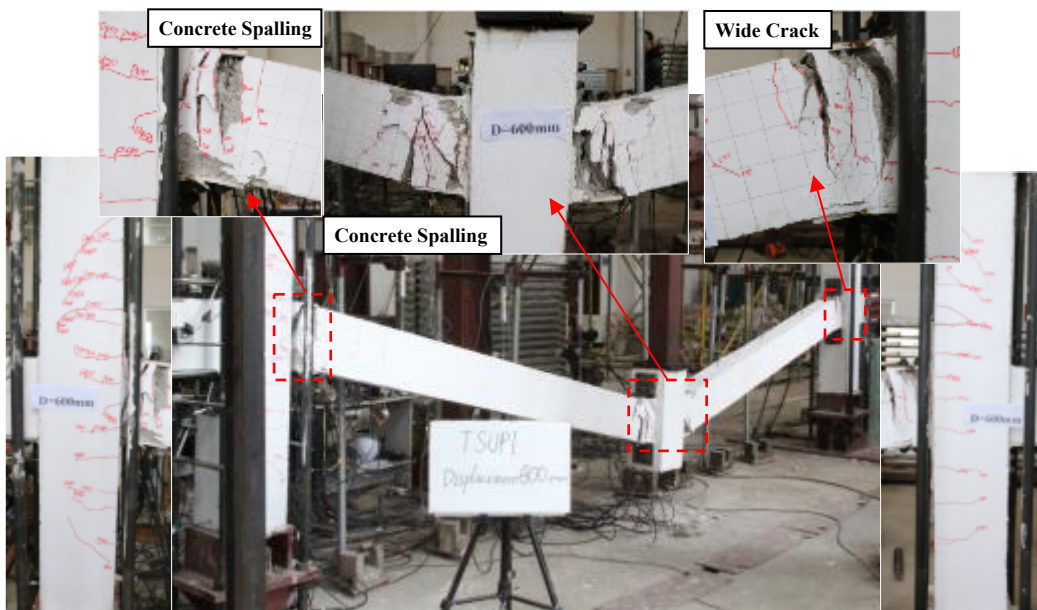
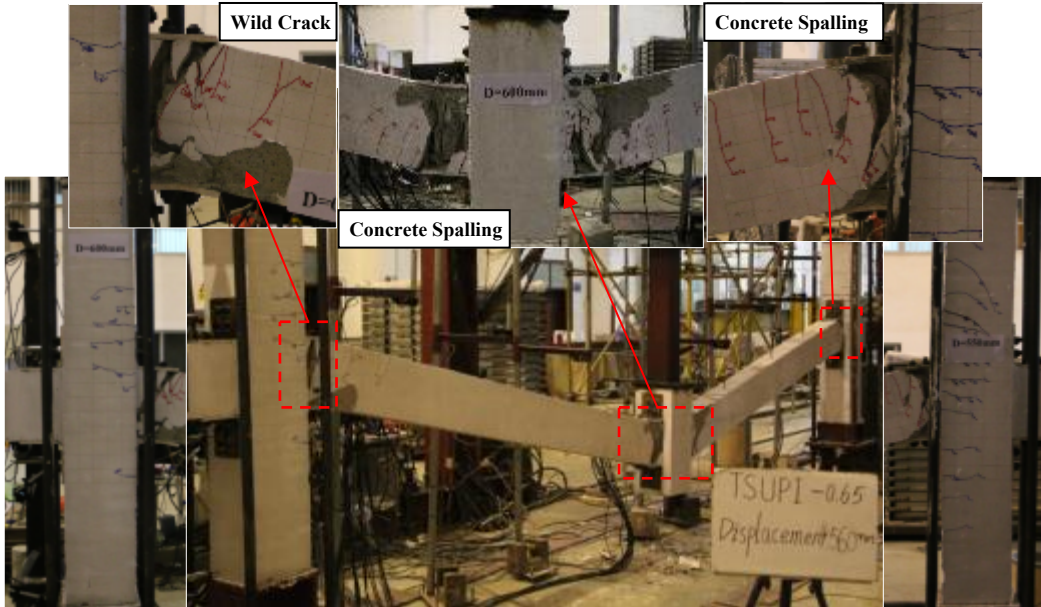


Fig. 13. Failure mode of TSUPI-0.4

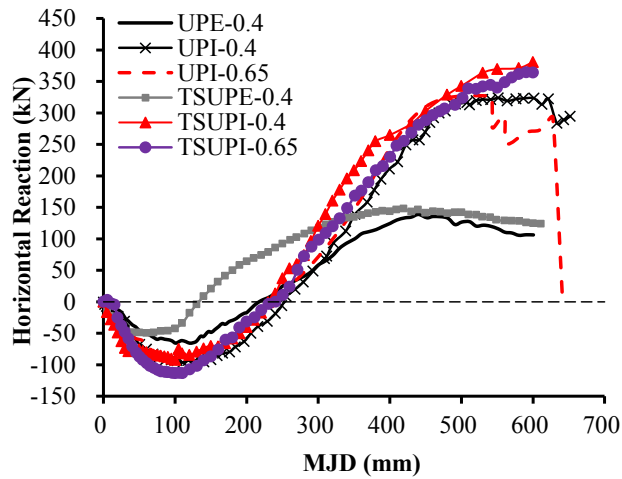
777
778
779
780
781
782
783
784
785
786
787
788
789

790
791
792



793
794
795

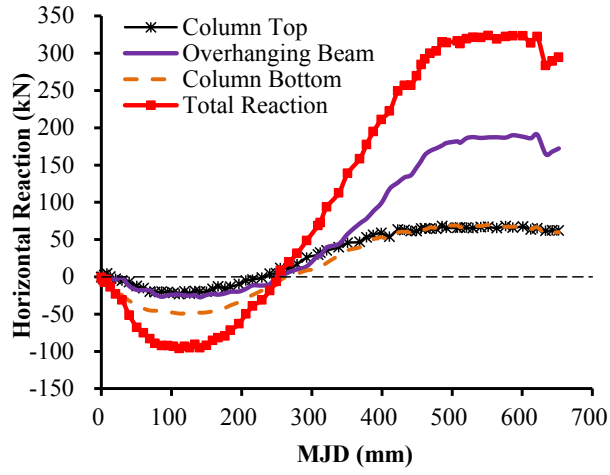
Fig. 14. Failure mode of TSUPI-0.65



796
797
798
799
800
801
802
803
804
805
806
807
808
809
810
811
812
813
814
815

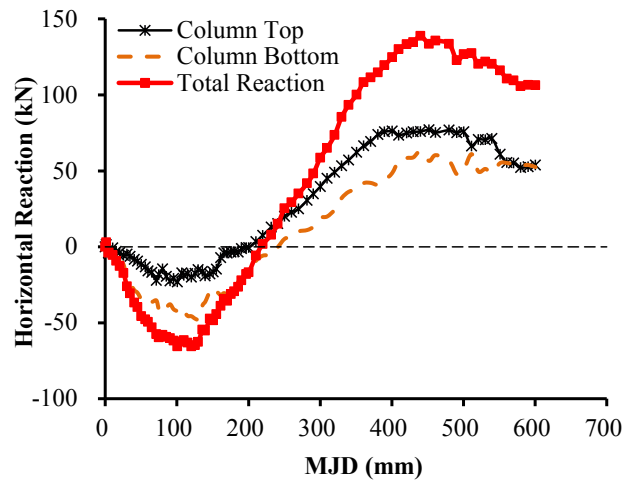
Fig. 15. Comparison of the horizontal reaction force versus MJD curves

816
817
818



(a)

819
820
821

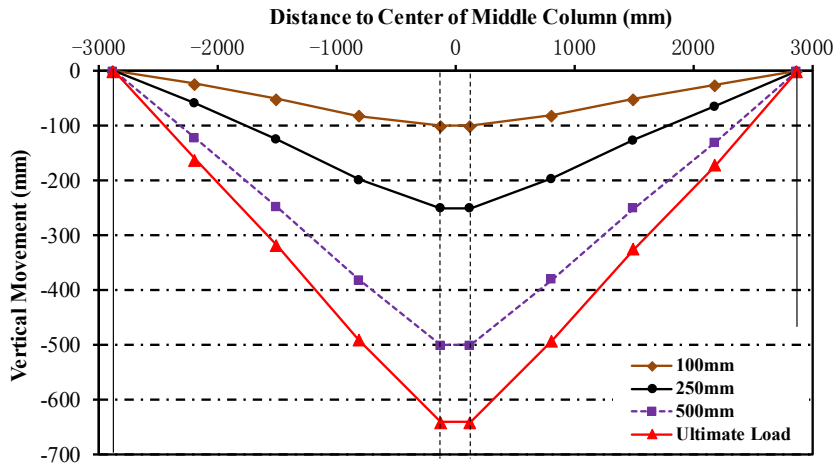


(b)

Fig. 16. Contribution of horizontal reaction force from each constraint: (a) UPI-0.4; (b) UPE-0.4

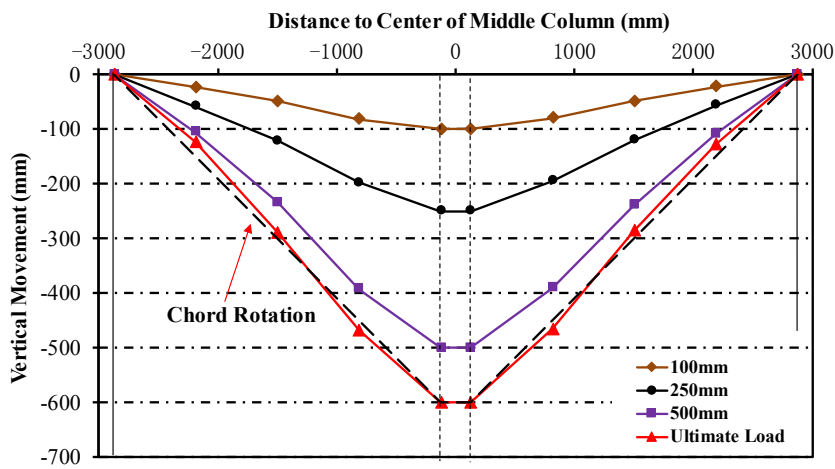
822
823
824
825
826
827
828
829
830
831
832
833
834
835
836
837
838
839
840
841
842
843
844

845
846



847
848
849

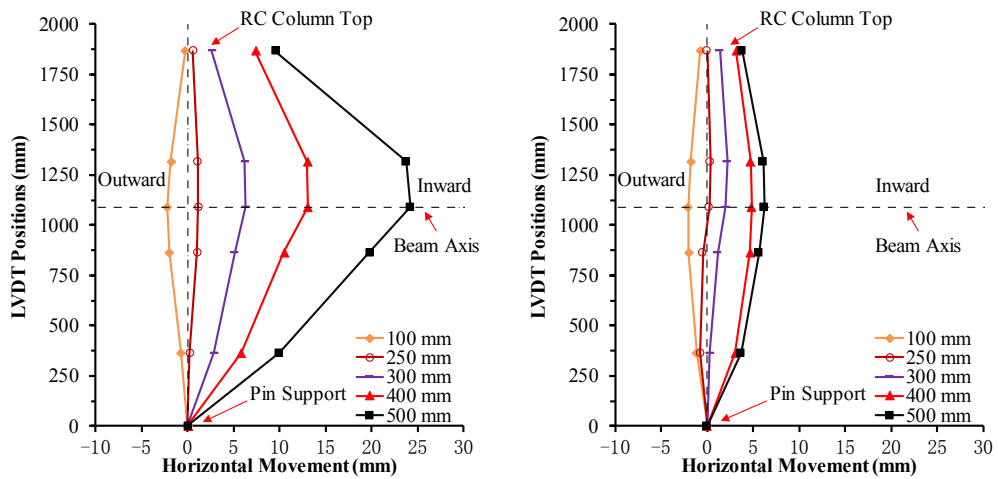
(a) UPI-0.65



850
851
852
853

(b) TSUPI-0.65

Fig. 17. Overall deflection of double-bay beam: (a) UPI-0.65; (b) TSUPI-0.65

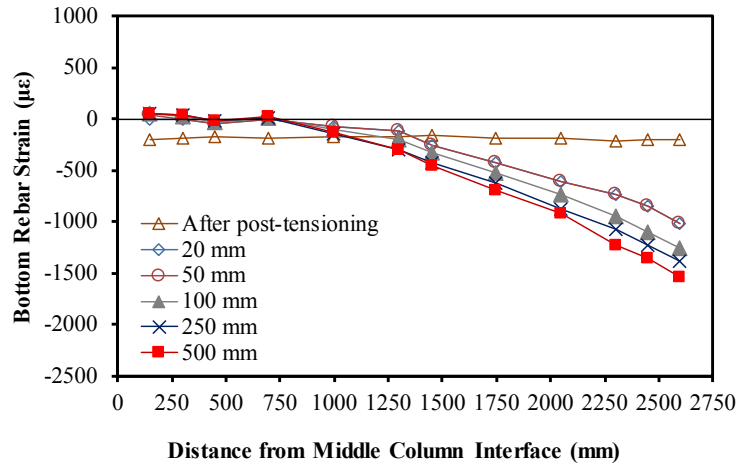


854
855
856
857
858
859
860

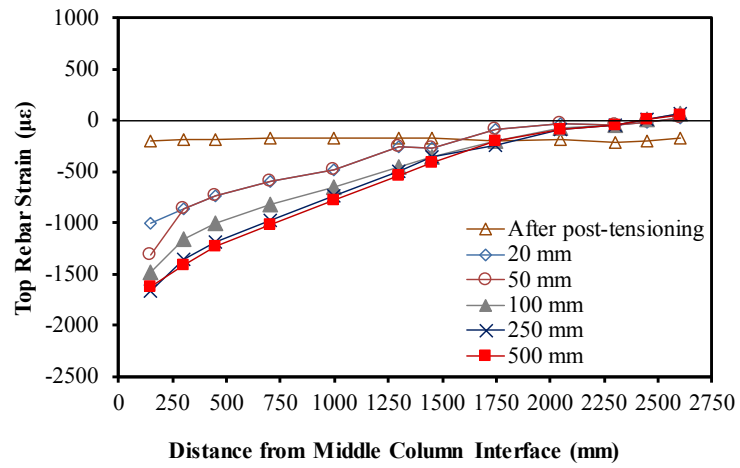
(a)

(b)

Fig. 18. Horizontal deformation in side column: (a) TSUPE-0.4; (b) TSUPI-0.4



(a)

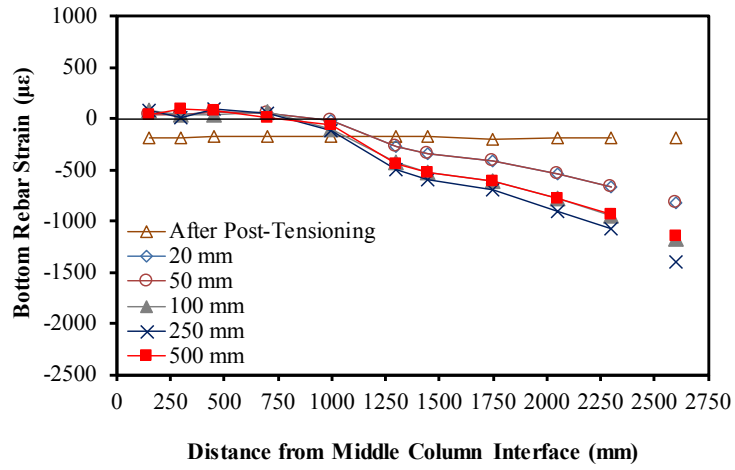


(b)

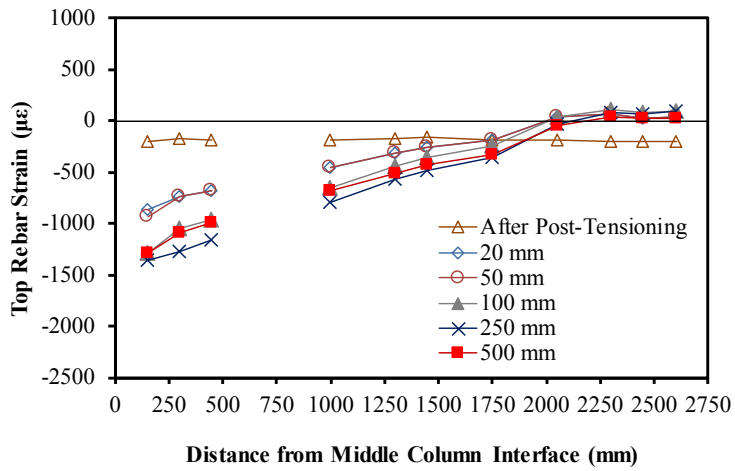
Fig. 19. Strain distribution in beam longitudinal reinforcement of UPE-0.4: (a) bottom rebar; (b) top rebar

861
862
863

864
865
866
867
868
869
870
871
872
873
874
875
876
877
878
879
880
881
882
883
884
885
886
887
888
889



(a)

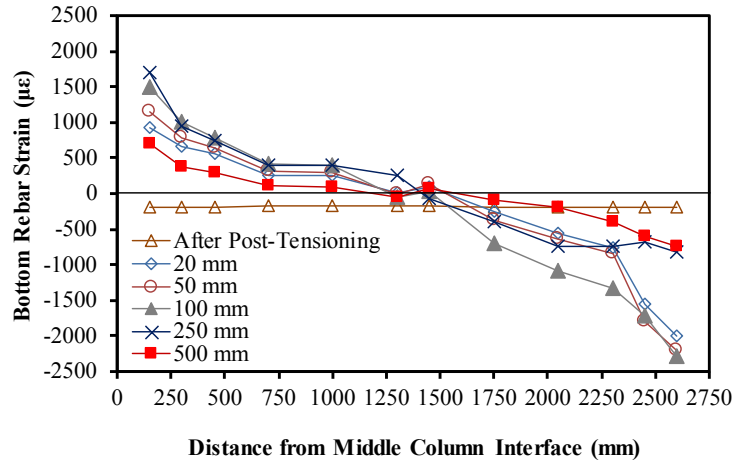


(b)

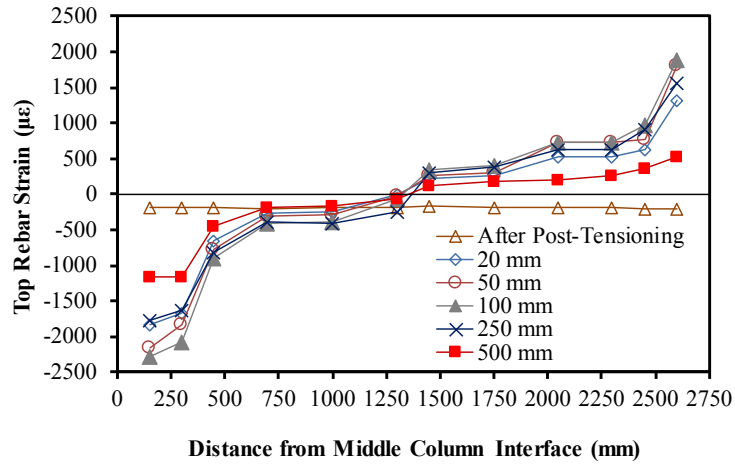
Fig. 20. Strain distribution in beam longitudinal reinforcement of UPI-0.4: (a) bottom rebar; (b) top rebar

890
891
892

893
894
895
896
897
898
899
900
901
902
903
904
905
906
907
908
909
910
911
912
913
914
915
916
917



(a)



(b)

Fig. 21. Strain distribution in beam longitudinal reinforcement of TSUPI-0.4: (a) bottom rebar; (b) top rebar

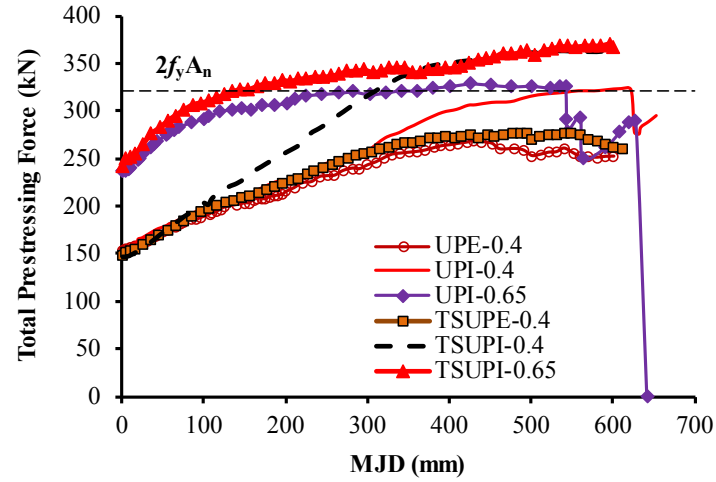
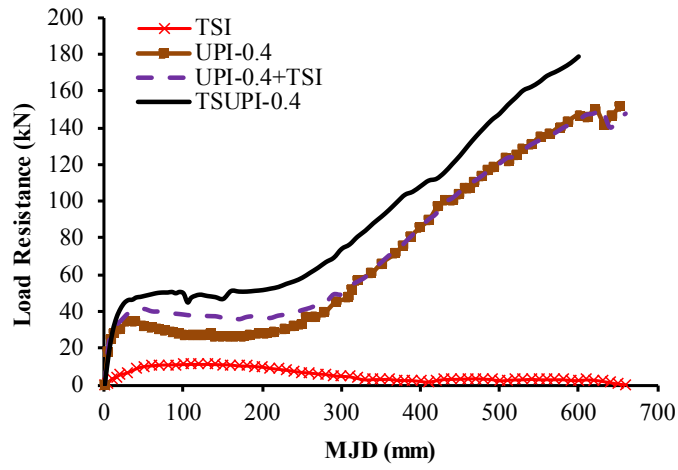


Fig. 22. Total prestressing forces-displacement relationship

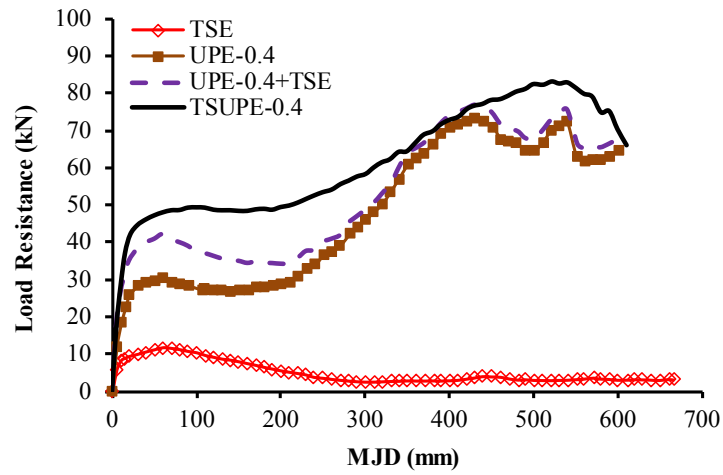
918
919
920

921
922
923
924

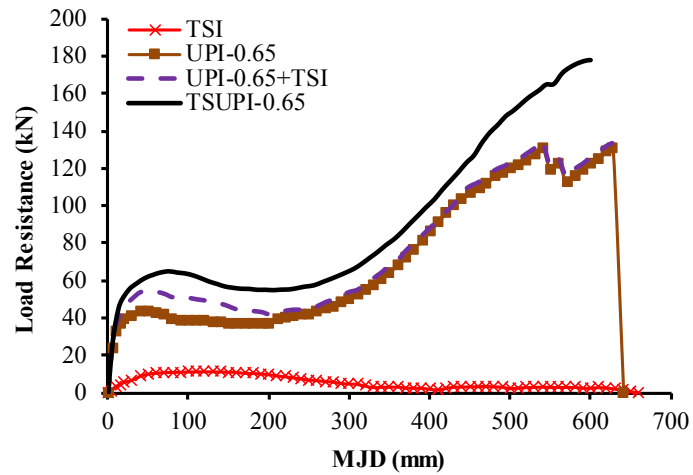
925
926
927
928
929
930
931
932
933



(a)



(b)



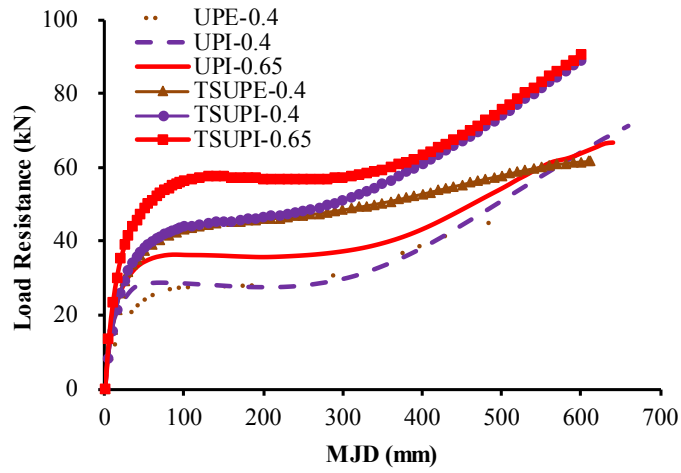
(c)

Fig. 23. Discussion of each design variable: (a) TSUPI-0.4; (b) TSUPE-0.4; (c) TSUPI-0.65

934
935

936
937

938
939
940
941
942
943
944
945
946
947
948
949
950



951
952
953
954
Fig. 24. Dynamic resistance of tested specimens

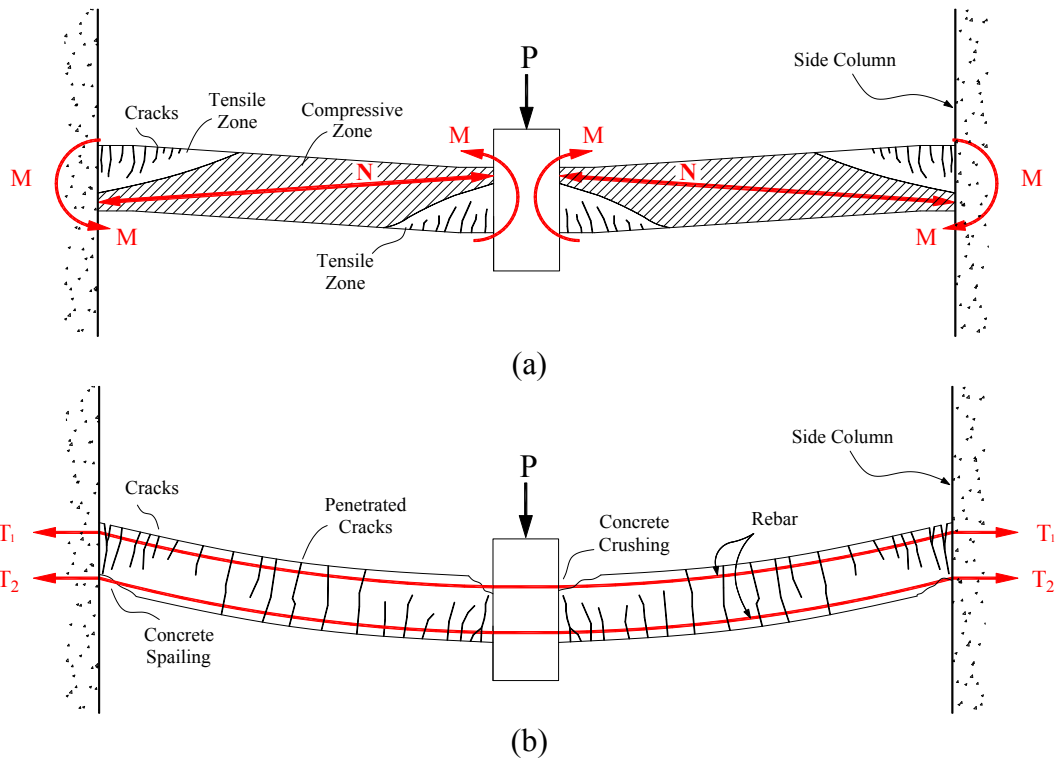
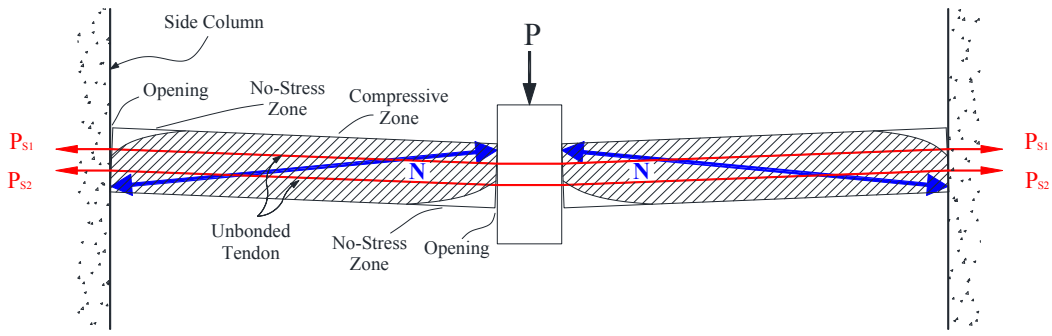
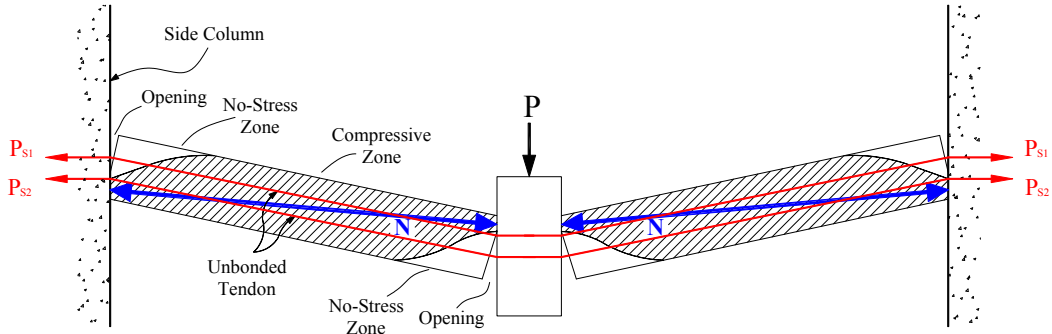


Fig. 25. Load resisting mechanism of RC structure: (a) compressive arch action; (b) tensile catenary action

976
977



(a)



(b)

Fig. 26. Load resisting mechanisms of specimens with unbonded post-tensioning connection: (a) small deformation; (b) MJD beyond one beam depth

978
979
980
981
982
983

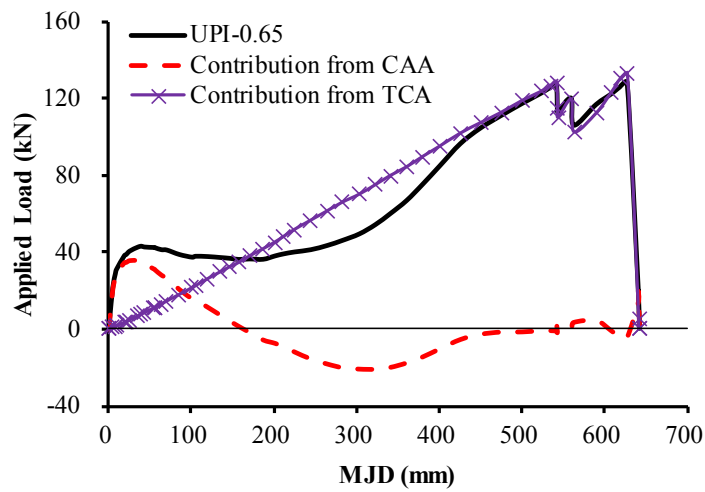


Fig. 27. Resistance decomposition of specimen UPI-0.65

984
985
986
987

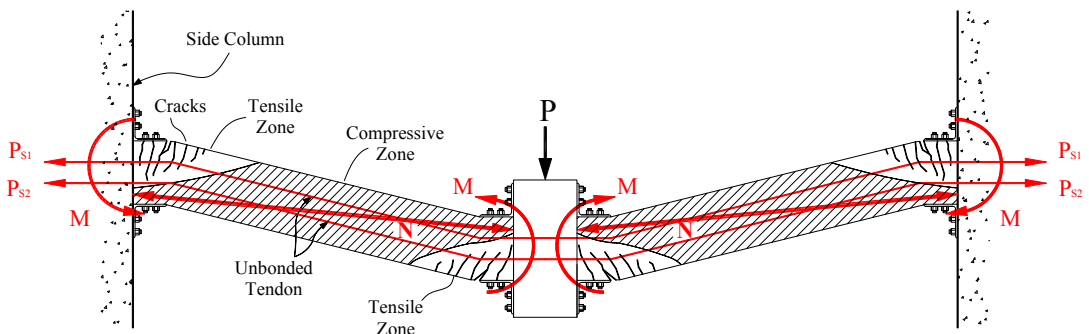


Fig. 28. Load resisting mechanism of specimens with hybrid connection

988
989
990